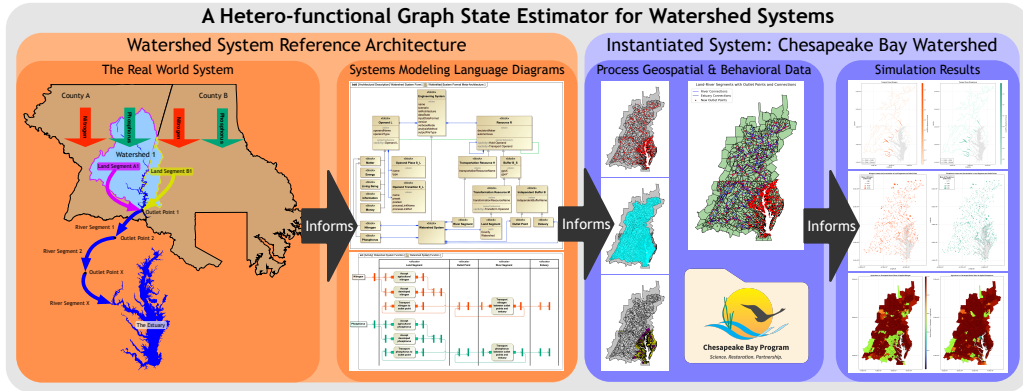


# Graphical Abstract

## A Hetero-functional Graph State Estimator for Watershed Systems: Application to the Chesapeake Bay

Megan S. Harris, John C. Little, Amro M. Farid



## Highlights

### **A Hetero-functional Graph State Estimator for Watershed Systems: Application to the Chesapeake Bay**

Megan S. Harris, John C. Little, Amro M. Farid

- Introduces an ontology-driven modeling framework for watershed systems
- Develops a reference architecture for watershed connectivity and nutrient application
- Extends a hetero-functional graph state estimator to infer nutrient flows
- Applies method to the Chesapeake Bay Watershed using geospatial and behavioral data
- Reveals system structure for future integration with governance and economic models

# A Hetero-functional Graph State Estimator for Watershed Systems: Application to the Chesapeake Bay

Megan S. Harris<sup>a</sup>, John C. Little<sup>a</sup>, Amro M. Farid<sup>b</sup>

<sup>a</sup>*Department of Civil and Environmental Engineering, Virginia Tech, Blacksburg, 24061, Virginia, United States*

<sup>b</sup>*School of Systems and Enterprises, Stevens Institute of Technology, Hoboken, 07030, New Jersey, United States*

---

## Abstract

Regional watersheds are complex systems of systems encompassing hydrology, land-use decision-making, estuarine ecological feedbacks, and overlapping governance jurisdictions. Their effective management underlies many modern societal challenges and therefore requires models that capture interdependencies between natural and institutional systems. Regional-specific models such as the Chesapeake Assessment Scenario Tool, used in this paper's case study, provide valuable nutrient estimates but rely on structurally opaque watershed routing that limits integration into broader systems-level analyses. This paper introduces a modeling framework for watershed systems. First, a region-independent reference architecture is developed. Second, the Weighted Least Squares Error Hetero-functional Graph State Estimator, an extension of Hetero-functional Graph Theory (HFGT), is adapted to estimate nutrient flows from uncertain data. The framework is demonstrated through instantiation in the Chesapeake Bay Watershed. By establishing a shared ontology grounded in Systems Modeling Language and HFGT, the approach enables integration of economic and governance systems to support sustainable watershed management.

*Keywords:* watershed modeling, Model-Based Systems Engineering (MBSE), Hetero-functional Graph Theory (HFGT), system of systems, Systems Modeling Language (SysML), nutrient transport

---

## 1. Introduction

The modern societal challenges reflected in the United Nations Sustainable Development Goals (SDGs) are inherently interconnected, arising from interactions among multiple systems of the Earth and society known as *systems of systems* (Defn. 1) [1, 2, 3]. These challenges depend on dynamic feedbacks between human and natural processes, including hydrology, agriculture, energy, infrastructure, economics, and governance [4, 5, 6]. Addressing them requires not only understanding each system individually, but also their interdependencies and how flows of water, energy, nutrients, and information move across disciplinary and spatial boundaries. Within hydrology, a wide range of process-based and data-driven models have been developed to describe these systems, yet persistent challenges remain in cross-system and cross-scale integration [7, 8, 9].

**Definition 1 – System of Systems:** 1) System of interest whose system elements are themselves systems; typically, these entail large-scale interdisciplinary problems with multiple, heterogeneous, distributed systems [10]. 2) Set of systems or system elements that interact to provide a unique capability that none of the constituent systems can accomplish on its own [11]. ■

Previous work by Harris et al. [12] demonstrated, through illustrative hydrological examples, how the integration of Model-Based Systems Engineering (MBSE) and Hetero-functional Graph Theory (HFGT) can reveal and formalize these cross-system dependencies within a unified ontology. Complementarily, Thompson and Farid [13] developed the Weighted Least Squares Error Hetero-functional Graph State Estimator (WLSEHFGSE), a generalized optimization and estimation framework for integrating heterogeneous and partially observed data. Together, these advances establish a foundation for applying MBSE and HFGT to real-world, multi-scale environmental systems.

This paper extends that foundation to larger watershed systems of systems spanning hydrology, estuarine ecology, agriculture, infrastructure, regional economics, and policy with a case study of the Chesapeake Bay Watershed (CBW). The CBW region is an ideal testbed for translating the MBSE–HFGT framework from illustrative systems to real-world applications based on its size, data availability, complexity, and economic and policy relevance.

The CBW spans six states and the District of Columbia and includes the largest estuary in the United States [14]. The estuary itself, the final

destination of watershed-routed water and nutrients, is one of the most comprehensively modeled and monitored ecosystems in the world [15, 16, 17]. Physiographic diversity from the Appalachians through the Piedmont to the Coastal Plain creates strong gradients in runoff generation, transport, and attenuation [16]. These interacting processes contribute to long-standing environmental degradation, including eutrophication and hypoxia [18, 19], and long-term declines in water quality [20]. This degradation impacts fishery productivity [21], public health [22], and water clarity valued by residents and tourists [23]. With ecosystem services valued at over \$100 billion annually [24], understanding the coupled dynamics of the CBW remains a regional and national priority.

Since 2017, the Chesapeake Assessment Scenario Tool (CAST) serves as the CBP’s official planning model for nutrient and sediment management [25, 15]. CAST aggregates land-based nutrient loads, applies empirical delivery factors, and simulates their delivery to the estuary, relying on decades of watershed model development [16, 26, 17]. However, CAST has three major limitations for system-of-systems modeling: 1. its internal routing structure is not explicitly represented [27], limiting transparency; 2. its logic is static and not designed for time-dependent simulation [27]; 3. it is only loosely coupled with estuarine models [15, 28], reducing its capacity to represent cross-domain interdependencies. As a result, researchers and decision-makers lack an extensible, scalable model of the Chesapeake Bay Watershed that can be embedded directly into system-of-systems analyses. These gaps motivate the development of an integrated modeling architecture that assimilates CAST data within the MBSE-HFGT framework.

### *1.1. Original Contribution*

This paper contributes a modeling framework for representing watershed systems with ultimate instantiation in the Chesapeake Bay Watershed region. The framework integrates open-source geospatial processing with an estimation methodology grounded in HFGT. First, the paper defines a generic watershed system under the HFGT meta-architecture. From there, watershed dynamics are derived as a generalization of the WLSEHFGSE [13], which extends the Hetero-functional Network Minimum Cost Flow (HFNMCf) formulation [29] by incorporating estimation error terms into the state transition constraints. This formulation enables the inference of unknown or partially observed flows from real-world data while preserving physical feasibility and structural consistency. The paper then instantiates this formulation for the

modeling suite of the Chesapeake Bay Watershed. A reproducible, Python-based pipeline constructs hetero-functional incidence tensors for the watershed for the WLSEHFGSE engineering state transition functions from publicly available geospatial data, including digital elevation models (DEMs), stream networks, river segment polygons, and estuarine boundaries. This approach explicitly identifies outlet points, resolves routing connections between river segments, and defines the spatial topology of the watershed consistent with the assumptions of CAST, but within a transparent format. CAST-derived exogenous data is then integrated to quantify nutrient flows throughout the watershed as part of the WLSEHFGSE measurement function.

Together in the instantiated system model, these structural and behavioral elements yield a unified representation of the Chesapeake Bay Watershed system. The hetero-functional incidence tensor of the CBW provides the spatial foundation for system network connectivity, while the functional model enables estimation of dynamic flows within a rigorous systems-engineering framework. In short, HFGT supplies the missing structural layer beneath CAST’s statistical emulator, aligning management-efficient scenario evaluation with a physically interpretable network model. Collectively, these contributions form a foundational step toward an extensible system of systems model of the Chesapeake Bay, one capable of bridging hydrology, economy, and policy within a shared computational ontology grounded in MBSE and HFGT.

### *1.2. Paper Outline*

The remainder of the paper is organized as follows. Section 2 details the methodological approach of the paper, including an overview of the Chesapeake Bay modeling suite and the HFGT meta-architecture, mathematical formulation, and existing applications. Subsection 2.3 then outlines the WLSEHFGSE, a generic optimization framework for estimating operand flows from uncertain data. Section 3 defines a reference architecture of generic watershed systems under the HFGT meta-architecture. Section 4 simplifies the WLSEHFGSE optimization model for generic watershed system simulation. Section 5 details the instantiation of the Chesapeake Bay Watershed modeling suite. First, Subsection 5.1 describes how geospatial data is used to create hetero-functional incidence tensors that explicitly route nutrients in the CBW for synthesis of the WLSEHFGSE state transition function. Subsection 5.2 describes the quantification of the WLSEHFGSE measurement

function using CAST data to exogenously define nutrient flows. From there, Section 6.1 presents the results and Section 6.2 discusses the practical implications of this work. Ultimately, Section 7 summarizes the contributions and outlines future directions.

## 2. Methodological Background

This section provides the methodological foundation for the proposed framework as applied to the Chesapeake Bay Watershed. Subsection 2.1 introduces CAST, the operational modeling system used by the Chesapeake Bay Program to estimate nutrient and sediment loads across the region. Subsection 2.2 presents MBSE and HFGT as a generalized mathematical formalism for representing and analyzing the structure and behavior of systems of systems. Building on this foundation, Subsection 2.3 defines the WLSEHFGSE as an optimization-based extension of HFGT that enables simulation and estimation of operand flows within systems instantiated under the HFGT meta-architecture. The methods presented in this paper draw on established work in watershed modeling and systems engineering. While this section summarizes the essential background knowledge required to follow the results, readers needing additional technical depth are referred to the cited sources.

### *2.1. The Chesapeake Bay Modeling Suite and the Chesapeake Assessment Scenario Tool (CAST)*

The Chesapeake Bay Program operates a highly integrated modeling suite that connects watershed, airshed, and estuary dynamics. The watershed component of this suite is operationalized in CAST, the publicly accessible, time-averaged system for estimating nitrogen, phosphorus, and sediment loads throughout the Chesapeake Bay Watershed [25, 15]. Geospatially, CAST partitions the region into land-river segments which are the intersection of county and watershed boundaries. The model produces annual Edge of Stream (EOS) and End of Tide (EOT) delivered loads aggregated by county [27]. Computationally, CAST functions as a statistically calibrated emulator: average-load functions, best management practice (BMP) effects, and delivery factors (land to water, stream, river) are derived from mechanistic model outputs, literature syntheses, and empirical fits to monitoring data [15]. For example, land-to-water and stream delivery were informed by USGS/SPARROW-style relations and empirical modeling [26, 30], while

river-to-bay delivery factors were constrained using the dynamic watershed-estuary model [15, 31].

From Phase 1, released in 1985, through Phase 5, released in 2010, the CBP watershed model was mechanistic and based in Hydrological Simulation Program - FORTRAN (HSPF) [16]. The model runs at hourly timesteps to simulate hydrology, sediment, and nutrient cycling across segments, with extensive calibration and linkage to a 3-D estuarine water-quality and sediment-transport model (WQSTM/CH3D-ICM) [16]. Foundational documentation spans the HSPF manuals and CBP watershed applications [32, 33], with airshed inputs provided via CMAQ/regression frameworks and cross-media coupling [34, 15]. This era preserved explicit routing and process couplings, where annual management metrics were produced by aggregating time-varying simulations.

Phase 6, released in 2017, created CAST, a time-averaged (annual) model that constrains the dynamic model to produce aggregated loads [15]. This redesign improved interpretability, computational speed, and alignment with management timelines while embedding multiple lines of evidence including mechanistic outputs, monitoring data, meta-analyses, and literature-based BMP efficiencies in a regression-style structure [15]. Empirical delivery factors based in SPARROW-type relations and literature-based coefficients were incorporated for consistency and transferability across the Chesapeake Bay Watershed's diverse physiographic settings [26, 30]. The estuary boundary loads and river delivery were checked against the dynamic watershed-estuary modeling system [31].

Because CAST collapses internal routing into delivery factors that route nutrients from land to river then directly to the estuary, it does not explicitly represent the upstream-downstream network topology present in the mechanistic HSPF lineage. This abstraction limits transparent representation of hydrologic connectivity, subwatershed processes, and strict mass conservation within the routing network [15]. Hood et al. emphasize needs for [15, 35]: 1. consistency of nutrient delivery across spatial and temporal scales, 2. more explicit subwatershed hydrologic depiction, 3. and greater spatial explicitness and mass conservation in the time-averaged suite to better quantify riparian/wetland source-sink behavior. They also highlight broader challenges facing the Chesapeake Bay Watershed modeling suite under anthropogenic change including climate-nutrient interactions, reinforcing the need for frameworks that accommodate cross-scale feedbacks, and evolving data streams [36, 37, 38, 28, 39, 40].

The MBSE-HFGT approach developed in this paper reconstructs the implicit flow structure of CAST as an explicit, mass-conserving network that connects land segments, rivers, and the estuary. By embedding delivery and BMP effects within a graph-theoretic representation, the paper: 1. restores upstream-downstream connectivity, 2. enforces accounting consistency across spatial scales, 3. and creates a scaffold for future extensions including incorporating nutrient partitioning between particulate and dissolved forms for tighter estuary coupling [31] and assimilating monitoring-based flux estimates to refine spatial variability and temporal trends [41].

Although the watershed component of the Chesapeake Bay modeling suite is rooted in a fully dynamic, HSPF-based hydrologic and water-quality model [32, 16], this paper deliberately focuses on CAST as the primary point of integration with the MBSE-HFGT framework. CAST is the operational tool used by managers and is openly accessible via a free web interface. Thus, CBP policy guides its structure, assumptions, and outputs. At the same time, CAST functions as a statistically calibrated emulator of the underlying HSPF lineage [15]. This makes CAST an ideal test bed for demonstrating how empirically calibrated, data-driven models can be systematically recast as explicit, mass-conserving network models within the HFGT meta-architecture. In future work, the resulting HFGT-based watershed representation can be further evaluated against both monitoring data and the original HSPF-based dynamic model, as well as coupled hydrologic-economic frameworks that build on HSPF-type process models [42, 43, 44].

## 2.2. Hetero-functional Graph Theory (HFGT) Meta-Architecture & Definitions

HFGT extends traditional graph theory by incorporating system functions, making it particularly suited for modeling complex, heterogeneous systems. It provides a formal means to represent what is broadly referred to as the *engineering system* (Def. 2). Engineering systems encompass both designed and natural systems including systems of systems (Defn. 1). Expressed in the language of systems engineering, systems of systems are a class of engineering systems. HFGT represents engineering systems through three primary ontological elements: *resources*, *processes*, and *operands*. Together, these elements form the foundation of HFGT’s meta-architecture.

**Definition 2 – Engineering System [45]:** 1. A class of systems characterized by a high degree of technical complexity, social intricacy, and elaborate processes aimed at fulfilling important functions in society, and 2. The term

engineering systems is also used to refer to the engineering discipline that designs, analyzes, verifies, and validates *engineering systems*. ■

**Definition 3 – System Operand [46]:** An asset or object  $l_i \in L$  that is operated on or consumed during the execution of a process. ■

**Definition 4 – System Process [47, 46]:** An activity  $p \in P$  that transforms or transports a predefined set of input operands into a predefined set of outputs. ■

**Definition 5 – System Resource [46]:** An asset or object  $r_v \in R$  that facilitates the execution of a process. ■

These elements are connected through *subject-verb-object* (SVO) sentences, where resources (subjects) realize processes (verbs) involving operands (objects) [46, 47]. In this framework, resources are elements that enable processes to occur, such as physical infrastructure, institutions, or environmental systems (Def. 5). Processes represent activities that transform or transport operands (Def. 4), while operands are the elements being acted upon, such as water in a hydrological model or data in a computational system (Def. 3). This SVO-based ontology provides an unambiguous and discipline-independent representation of system functionality. For example, the statement “*Resource  $r_v$  performs process  $p_w$  on operand  $l_i$* ” explicitly defines a functional interaction within the system, ensuring semantic and structural consistency across domains.

The organization of these elements within HFGT is formalized using a *Reference Architecture* (RA). The RA categorizes both system form and function within a unified ontology, facilitating model consistency and extensibility. In practice, this structure is visualized using SysML diagrams. Block Definition Diagrams (BDD) define system form by classifying and relating resources, while Activity Diagrams (ACT) define system function by mapping processes to the resources that perform them. Together, these diagrams support interoperability and traceability across disciplines.

For analytical clarity, resources and processes are further classified. The set of resources,  $R = M \cup B \cup H$ , is divided into transformation resources ( $M$ ), independent buffers ( $B$ ), and transportation resources ( $H$ ) (Def. 5). Buffers, collectively represented as  $B_S = M \cup B$ , encompass resources capable of storing or transforming operands at specific spatial locations [48, 49]. Processes ( $P$ ) are similarly divided into transformation processes ( $P_\mu$ ), which modify operands within the system, and refined transportation processes ( $P_\eta$ ), which represent combined movement and holding behaviors (Def. 4).

**Definition 6 – Buffer [48, 49]:** A resource  $r_v \in R$  is a buffer  $b_s \in B_S$  iff it is capable of storing or transforming one or more operands at a unique location in space. ■

Finally, HFGT introduces the concept of *capabilities*, which specify the actions that a resource is able to perform. A capability is defined as a resource  $r_v$  executing a process  $p_w$  to produce specific outputs (Def. 5, Def. 4). These capabilities are expressed in the form: “*Resource  $r_v$  does process  $p_w$ ,*” providing a measurable way to represent system functionality. Figures 1 and 2 illustrate this form and function within the HFGT meta-architecture.

**Definition 7 – Capability [48, 49, 50]:** An action  $e_{vw} \in \mathcal{E}_S$  (in the SysML sense) defined by a system process  $p_w \in P$  being executed by a resource  $r_v \in R$ . ■

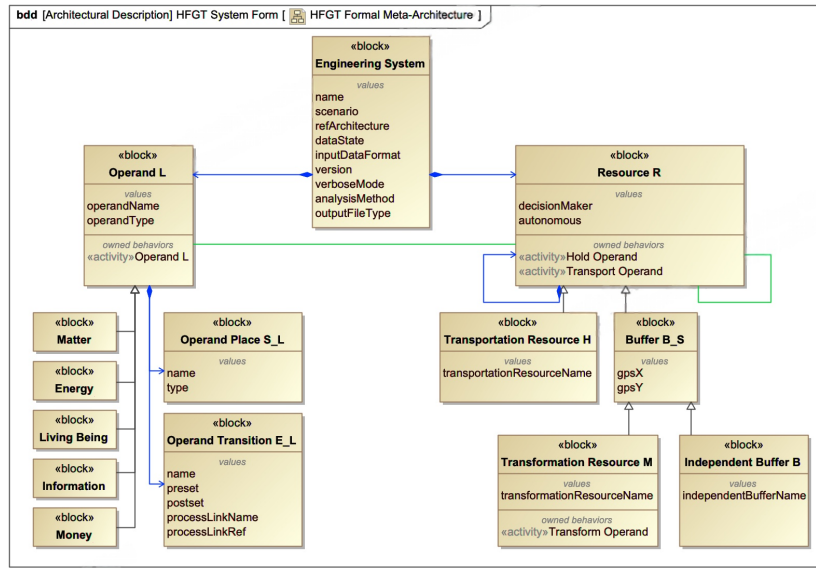


Figure 1: A SysML Block Definition Diagram of the System Form of the Engineering System Meta-Architecture. Adapted from [48].

The engineering system meta-architecture stated in SysML must be instantiated and ultimately transformed into the associated real world, instantiated model. To that end, the positive and negative hetero-functional incidence tensors (HFIT) are introduced to describe the flow of operands through buffers and capabilities.

**Definition 8 – The Negative  $3^{rd}$  Order Hetero-functional Incidence**

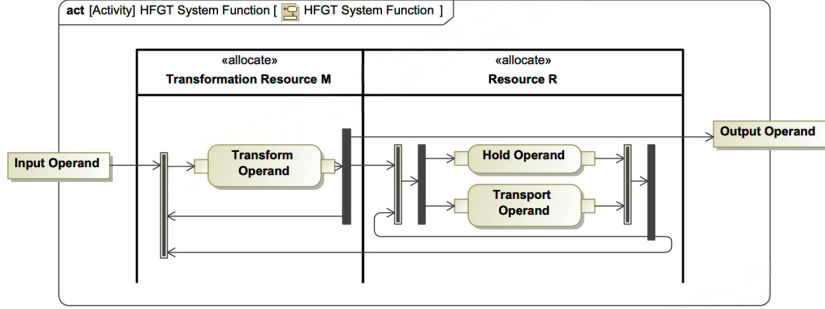


Figure 2: A SysML Activity Diagram of the System Function of the Engineering System Meta-Architecture. Adapted from [48].

**Tensor (HFIT  $\widetilde{\mathcal{M}}_\rho^-$  [49]):** The negative hetero-functional incidence tensor  $\widetilde{\mathcal{M}}_\rho^- \in \{0, 1\}^{|L| \times |B_S| \times |\mathcal{E}_S|}$  is a third-order tensor whose element  $\widetilde{\mathcal{M}}_\rho^-(i, y, \psi) = 1$  when the system capability  $\epsilon_\psi \in \mathcal{E}_S$  pulls operand  $l_i \in L$  from buffer  $b_{s_y} \in B_S$ . ■

**Definition 9 – The Positive 3<sup>rd</sup> Order Hetero-functional Incidence Tensor (HFIT  $\widetilde{\mathcal{M}}_\rho^+$  [49]):** The positive hetero-functional incidence tensor  $\widetilde{\mathcal{M}}_\rho^+ \in \{0, 1\}^{|L| \times |B_S| \times |\mathcal{E}_S|}$  is a third-order tensor whose element  $\widetilde{\mathcal{M}}_\rho^+(i, y, \psi) = 1$  when the system capability  $\epsilon_\psi \in \mathcal{E}_S$  injects operand  $l_i \in L$  into buffer  $b_{s_y} \in B_S$ . ■

These incidence tensors are straightforwardly “matricized” to form 2<sup>nd</sup> Order Hetero-functional Incidence Matrices  $M = M^+ - M^-$  with dimensions  $|L| |B_S| \times |\mathcal{E}|$ . Consequently, the supply, demand, transportation, storage, transformation, assembly, and disassembly of multiple operands in distinct locations over time can be described by an Engineering System Net and its associated State Transition Function [51].

**Definition 10 – Engineering System Net [51]:** An elementary Petri net  $\mathcal{N} = \{S, \mathcal{E}_S, M, W, Q\}$ , where

- $S$  is the set of places with size:  $|L| |B_S|$ ,
- $\mathcal{E}_S$  is the set of transitions with size:  $|\mathcal{E}|$ ,
- $M$  is the set of arcs, with the associated incidence matrices:  $M = M^+ - M^-$ ,

- $W$  is the set of weights on the arcs, as captured in the incidence matrices,
- $Q = [Q_B; Q_E]$  is the marking vector for both the set of places and the set of transitions.

■

**Definition 11 – Engineering System Net State Transition Function [51]:** The state transition function of the engineering system net  $\Phi()$  is:

$$Q[k+1] = \Phi(Q[k], U^-[k], U^+[k]) \quad \forall k \in \{1, \dots, K\} \quad (1)$$

where  $k$  is the discrete time index,  $K$  is the simulation horizon,  $Q = [Q_B; Q_E]$ ,  $Q_B$  has size  $|L||B_S| \times 1$ ,  $Q_E$  has size  $|\mathcal{E}_S| \times 1$ , the input firing vector  $U^-[k]$  has size  $|\mathcal{E}_S| \times 1$ , and the output firing vector  $U^+[k]$  has size  $|\mathcal{E}_S| \times 1$ .

$$Q_B[k+1] = Q_B[k] + M^+U^+[k]\Delta T - M^-U^-[k]\Delta T \quad (2)$$

$$Q_E[k+1] = Q_E[k] - U^+[k]\Delta T + U^-[k]\Delta T \quad (3)$$

where  $\Delta T$  is the duration of the simulation time step. ■

Here, it is important to recognize that the engineering system net state transition function is a restatement of a mass balance or continuity law in engineering (Equation 2) [51]. The engineering system net includes parameters describing the storage of operands within buffers and their flows into and out of those buffers. For the CBW with a land segment as the control volume, this includes the volume within the control volume, the flow of nutrients into the control volume, and the flow of nutrients out of the control volume.

In addition to the engineering system net, in HFGT, each operand can have its own state and evolution. This behavior is described by an Operand Net and its associated State Transition Function for each operand.

**Definition 12 – Operand Net [52, 48, 53, 54]:** Given operand  $l_i$ , an elementary Petri net  $\mathcal{N}_{l_i} = \{S_{l_i}, \mathcal{E}_{l_i}, M_{l_i}, W_{l_i}, Q_{l_i}\}$  where

- $S_{l_i}$  is the set of places describing the operand's state.
- $\mathcal{E}_{l_i}$  is the set of transitions describing the evolution of the operand's state.
- $M_{l_i} \subseteq (S_{l_i} \times \mathcal{E}_{l_i}) \cup (\mathcal{E}_{l_i} \times S_{l_i})$  is the set of arcs, with the associated incidence matrices:  $M_{l_i} = M_{l_i}^+ - M_{l_i}^- \quad \forall l_i \in L$ .

- $W_{l_i} : M_{l_i}$  is the set of weights on the arcs, as captured in the incidence matrices  $M_{l_i}^+, M_{l_i}^- \quad \forall l_i \in L$ .
- $Q_{l_i} = [Q_{S_{l_i}}; Q_{\mathcal{E}_{l_i}}]$  is the marking vector for both the set of places and the set of transitions.

■

**Definition 13 – Operand Net State Transition Function [52, 48, 53, 54]:** The state transition function of each operand net  $\Phi_{l_i}()$  is:

$$Q_{l_i}[k+1] = \Phi_{l_i}(Q_{l_i}[k], U_{l_i}^-[k], U_{l_i}^+[k]) \quad \forall k \in \{1, \dots, K\} \quad i \in \{1, \dots, L\} \quad (4)$$

where  $Q_{l_i} = [Q_{S_{l_i}}; Q_{\mathcal{E}_{l_i}}]$ ,  $Q_{S_{l_i}}$  has size  $|S_{l_i}| \times 1$ ,  $Q_{\mathcal{E}_{l_i}}$  has size  $|\mathcal{E}_{l_i}| \times 1$ , the input firing vector  $U_{l_i}^-[k]$  has size  $|\mathcal{E}_{l_i}| \times 1$ , and the output firing vector  $U_{l_i}^+[k]$  has size  $|\mathcal{E}_{l_i}| \times 1$ .

$$Q_{S_{l_i}}[k+1] = Q_{S_{l_i}}[k] + M_{l_i}^+ U_{l_i}^+[k] \Delta T - M_{l_i}^- U_{l_i}^-[k] \Delta T \quad (5)$$

$$Q_{\mathcal{E}_{l_i}}[k+1] = Q_{\mathcal{E}_{l_i}}[k] - U_{l_i}^+[k] \Delta T + U_{l_i}^-[k] \Delta T \quad (6)$$

■

Here, HFGT introduces operand nets and their associated state transition functions. This functionality does not always have a direct counterpart in watershed systems. Other application domains, most notably production systems [54, 52, 55] and healthcare systems [56, 53, 57] respectively have products and patients as operands with often very complex operand state evolution. Such operand state behavior is predicated on a Lagrangian view rather than Eulerian view of the system [58]. Therefore, water system models – which adopt an Eulerian view – do not make use of operand nets and their state transition functions.

Together, these tensors and the Engineering System Net form the computational foundation of HFGT and can be directly instantiated from real-system data using the HFGT Toolbox [59]. The HFGT toolbox algorithmically translates SysML-based representations of system form and function into data structures for simulation, bridging graphical, mathematical, and computational domains.

### 2.3. *Weighted Least Squares Error Hetero-functional Graph State Estimation (WLSEHFGSE)*

HFGT formally characterizes the structure and dynamics of engineered and natural systems through the HFNMCf problem [51]. The HFNMCf formulation defines the flow and storage of multiple operands across heterogeneous system functions, optimizing their transportation, transformation, and accumulation in discrete time. It serves as the computational foundation linking the HFGT structural outputs, such as the hetero-functional incidence tensor and capability matrices, to system-level behavioral modeling.

Building on this foundation, the WLSEHFGSE problem extends the HFNMCf problem by explicitly incorporating uncertainty in exogenous data [13]. Where the HFNMCf optimizes deterministic operand flows under known boundary conditions, the WLSEHFGSE introduces statistical error terms into the equality constraints governing state transitions and measurements (Eqs. 7j–7k) [13]. This generalization enables the inference of unknown or partially observed flows from imperfect or incomplete data while maintaining the topological and physical consistency imposed by the HFGT structure [13]. The WLSEHFGSE thus transforms the HFNMCf from a purely optimization-based flow model into a generalized estimation framework suitable for reconstructing real-world systems, such as the CBW, from empirical data.

$$\min Z = \sum_{k=1}^{K-1} f_k(x[k], y[k]) \quad (7a)$$

subject to:

$$-Q_B[k+1] + Q_B[k] + M^+U^+[k]\Delta T - M^-U^-[k]\Delta T = 0 \quad \forall k \in \{1, \dots, K\} \quad (7b)$$

$$-Q_{\mathcal{E}}[k+1] + Q_{\mathcal{E}}[k] - U^+[k]\Delta T + U^-[k]\Delta T = 0 \quad \forall k \in \{1, \dots, K\} \quad (7c)$$

$$-U_{\psi}^+[k+k_{d\psi}] + U_{\psi}^-[k] = 0 \quad \begin{array}{l} \forall k \in \{1, \dots, K\} \\ \forall \psi \in \{1, \dots, \mathcal{E}_S\} \end{array} \quad (7d)$$

$$-Q_{SL_i}[k+1] + Q_{SL_i}[k] + M_{l_i}^+U_{l_i}^+[k]\Delta T - M_{l_i}^-U_{l_i}^-[k]\Delta T = 0 \quad \begin{array}{l} \forall k \in \{1, \dots, K\} \\ \forall i \in \{1, \dots, |L|\} \end{array} \quad (7e)$$

$$-Q_{\mathcal{E}l_i}[k+1] + Q_{\mathcal{E}l_i}[k] - U_{l_i}^+[k]\Delta T + U_{l_i}^-[k]\Delta T = 0 \quad \begin{array}{l} \forall k \in \{1, \dots, K\} \\ \forall i \in \{1, \dots, |L|\} \end{array} \quad (7f)$$

$$-U_{xl_i}^+[k+k_{dxl_i}] + U_{xl_i}^-[k] = 0 \quad \begin{array}{l} \forall k \in \{1, \dots, K\} \\ \forall x \in \{1, \dots, |\mathcal{E}l_i|\} \\ \forall l_i \in \{1, \dots, |L|\} \end{array} \quad (7g)$$

$$U_L^+[k] - \hat{\Lambda}^+U^+[k] = 0 \quad \forall k \in \{1, \dots, K\} \quad (7h)$$

$$U_L^-[k] - \hat{\Lambda}^-U^-[k] = 0 \quad \forall k \in \{1, \dots, K\} \quad (7i)$$

$$\begin{bmatrix} D_{Up} & \mathbf{0} \\ \mathbf{0} & D_{Un} \end{bmatrix} \begin{bmatrix} U^+ \\ U^- \end{bmatrix} = \begin{bmatrix} C_{Up} + \mathcal{E}_{Up} \\ C_{Un} + \mathcal{E}_{Un} \end{bmatrix} \quad (7j)$$

$$\begin{bmatrix} E_{Lp} & \mathbf{0} \\ \mathbf{0} & E_{Ln} \end{bmatrix} \begin{bmatrix} U_{l_i}^+ \\ U_{l_i}^- \end{bmatrix} = \begin{bmatrix} F_{Lpi} + \mathcal{E}_{Lpi} \\ F_{Lni} + \mathcal{E}_{Lni} \end{bmatrix} \quad (7k)$$

$$[Q_B; Q_{\mathcal{E}}; Q_{SL}] [1] = [C_{B1}; C_{\mathcal{E}1}; C_{SL1}] \quad (7l)$$

$$[Q_B; Q_{\mathcal{E}}; Q_{SL}; U^-; U_L^-] [K+1] = [C_{BK}; C_{\mathcal{E}K}; C_{SLK}; \mathbf{0}; \mathbf{0}] \quad (7m)$$

$$D_{CP}X \leq E_{CP} \quad (7n)$$

$$g(X, Y) = 0 \quad (7o)$$

where  $X = [x[1]; \dots; x[K]]$  is the vector of primary decision variables and  $Y = [y[1]; \dots; y[K]]$  is the vector of auxiliary decision variables at time  $k$ . The vector of primary decision variables  $X = [x[1]; \dots; x[K]]$  specifically includes the measurement errors of exogenous data in  $\mathcal{E}_{Up}, \mathcal{E}_{Un}, \mathcal{E}_{Lp}, \mathcal{E}_{Ln}$ .

$$x[k] = [Q_B; Q_\varepsilon; Q_{SL}; Q_{\varepsilon L}; U^-; U^+; U_L^-; U_L^+; \mathcal{E}_{Up}; \mathcal{E}_{Un}; \mathcal{E}_{Lp}; \mathcal{E}_{Ln}] [k] \quad \forall k \in \{1, \dots, K\} \quad (8)$$

### 2.3.1. Objective Function

In Eq. 7a,  $Z$  is a convex objective function separable in discrete time steps  $k$ . Most commonly, a quadratic time-varying function is used.

$$Z_{QP} = \sum_{k=1}^{K-1} [x; y]^T [k] F_{QP}[k] [x; y][k] + f_{QP}[k] [x; y][k] \quad (9)$$

where the time-varying matrix  $F_{QP}[k]$  is assumed to be a positive semi-definite, diagonal, quadratic coefficient matrix, and the time-varying vector  $f_{QP}[k]$  is a linear coefficient matrix.

### 2.3.2. Equality Constraints

- Equations 7b and 7c describe the state transition function of an engineering system net (Defn 10 & 11).
- Equation 7d is the engineering system net transition duration constraint where the end of the  $\psi^{th}$  transition occurs  $k_{d\psi}$  time steps after its beginning.
- Equations 7e and 7f describe the state transition function of each operand net  $\mathcal{N}_{l_i}$  (Defn. 12 & 13) associated with each operand  $l_i \in L$ .
- Equation 7g is the operand net transition duration constraint where the end of the  $x^{th}$  transition occurs  $k_{dx_{l_i}}$  time steps after its beginning.
- Equations 7h and 7i are synchronization constraints that couple the input and output firing vectors of the engineering system net to the input and output firing vectors of the operand nets respectively.  $U_L^-$  and  $U_L^+$  are the vertical concatenations of the input and output firing

vectors  $U_{l_i}^-$  and  $U_{l_i}^+$  respectively.

$$U_L^-[k] = \left[ U_{l_1}^-; \dots; U_{l_{|L|}}^- \right] [k] \quad (10)$$

$$U_L^+[k] = \left[ U_{l_1}^+; \dots; U_{l_{|L|}}^+ \right] [k] \quad (11)$$

- Equations 7j and 7k are boundary conditions. Eq. 7j is a boundary condition constraint that allows some of the engineering system net firing vectors decision variables to be set to an exogenous constant. Eq. 7k does the same for the operand net firing vectors. Note that Equations 7j introduce measurement error variables  $\mathcal{E}_{Up}, \mathcal{E}_{Un}, \mathcal{E}_{Lp}, \mathcal{E}_{Ln}$ . Furthermore, Equations 7j and 7k introduce the concatenated vectors  $U^+ = [U^+[1]; \dots; U^+[K]]$ ,  $U^- = [U^-[1]; \dots; U^-[K]]$ ,  $U_{l_i}^+ = [U_{l_i}^+[1]; \dots; U_{l_i}^+[K]]$ , and  $U_{l_i}^- = [U_{l_i}^-[1]; \dots; U_{l_i}^-[K]]$ . This allows these equations to introduce exogenous data that spans multiple time steps.
- Equations 7l and 7m are the initial and final conditions of the engineering system net and the operand nets where  $Q_{SL}$  is the vertical concatenation of the place marking vectors of the operand nets  $Q_{Sl_i}$ .

$$Q_{SL}^-[k] = \left[ Q_{Sl_1}^-; \dots; U_{Sl_{|L|}}^- \right] [k] \quad (12)$$

$$U_{SL}^+[k] = \left[ U_{Sl_1}^+; \dots; U_{Sl_{|L|}}^+ \right] [k] \quad (13)$$

### 2.3.3. Inequality Constraints

$D_{QP}()$  and vector  $E_{QP}$  in Equation 7n place capacity constraints on the vector of primary decision variables at each time step:

$$x[k] = [Q_B; Q_E; Q_{SL}; Q_{EL}; U^-; U^+; U_L^-; U_L^+] [k] \quad \forall k \in \{1, \dots, K\}.$$

### 2.3.4. Device Model Constraints

$g(X, Y)$  and  $h(Y)$  are a set of device model functions whose presence and nature depend on the specific problem application. They can not be further elaborated until the application domain and its associated capabilities are identified.

The generic structure of HFGT has enabled its application across diverse engineered and socio-environmental domains. Prior studies have applied

HFGT to multi-modal and integrated energy networks [60, 61, 13, 62], the structural resilience of electric power systems [63, 64], interdependent smart city infrastructures [65, 66, 67], personalized healthcare delivery systems [68, 69], and reconfigurable manufacturing supply networks [70, 71]. These applications demonstrate the extensibility of the HFGT meta-architecture across systems with complex physical, functional, and informational dependencies.

This paper employs the WLSEHFGSE, an extension of the HFNMCFC formulation that admits measurement error in exogenously defined data [13]. A previous formulation for small hydrological systems simplified the HFNMCFC equations to model nitrogen flow through land segments, lakes, and rivers [12]. The work here builds on that existing reference architecture for hydrological systems and adapts it to represent large-scale watershed systems such as the Chesapeake Bay Watershed.

### **3. Applying the HFGT Meta-Architecture and Definitions to Watershed Systems**

This section applies the HFGT meta-architecture and definitions introduced in Section 2 to watershed systems. Subsection 3.1 develops a watershed BDD that is a specialization of the HFGT meta-architecture BDD shown in Fig. 1, and Subsection 3.2 develops an ACT that is a specialization of the HFGT meta-architecture ACT shown in Fig. 2. These graphical depictions together make up a watershed RA that allows the application in Subsection 3.3 of the definitions from Subsection 2.2. The goal is to represent the application and transport of nutrients, specifically nitrogen and phosphorus, which strongly influence aquatic ecosystem health.

Informed by CAST, the generic structure of watershed systems is visualized in Fig. 3. These systems include land segments, outlet points, river segments, and the estuary. The watershed system nutrient dynamics depend on three interacting domains: land use, watershed, and economic. On the economic side, nutrients are applied as fertilizer or manure for crop production, as a by product of animal husbandry, or industrial processes [27]. From a data perspective, these applications are reported at the county scale [27]. Land use characteristics then influence nutrient fate. For example, highly developed land facilitates runoff with limited infiltration, leading to higher nutrient concentrations in surface water. Finally, subwatersheds of varying size route water from any point on the land within their boundary to an

outlet point in the river network [27]. This river network accumulates flows across increasing stream orders, ultimately discharging into the estuary [27].

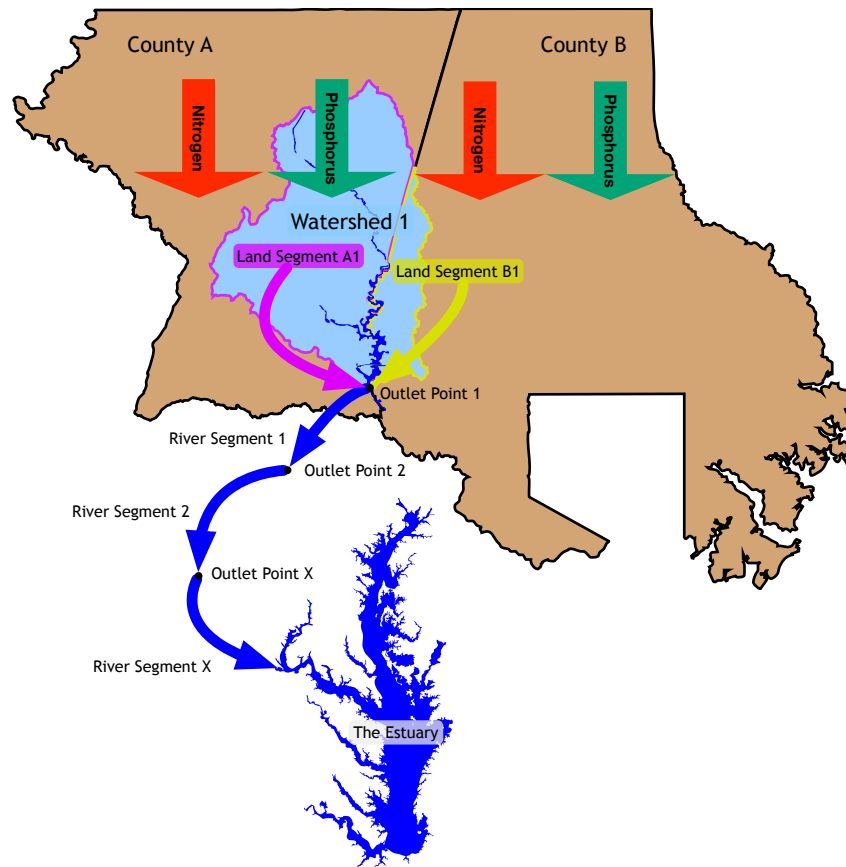


Figure 3: Schematic representation of nutrient flow across land segments, defined as the intersection of watershed and county boundaries. Nutrient loads are distributed from county totals across all nested land segments, aggregated at the watershed level, and routed downstream toward the estuary. The Liberty Dam Watershed is shown as an example, with Carroll County (A) and Baltimore County (B) highlighted [25].

### 3.1. Block Definition Diagram for a Generic Watershed System

This paper establishes watershed systems as a distinct class of engineering systems by defining a watershed BDD (Fig.4) under the engineering system meta-architecture BDD (Fig.1). This watershed system is a class of engineering system whose form is summarized to include the following: 1. land segments, represented by polygons defined by unique combinations

of county and river segment, 2. outlet points, where all land segments within a watershed drain, 3. river segments, which link outlet points to their next downstream outlet point, 4. estuaries, where watershed flows discharge, and 5. nutrients, nitrogen and phosphorus, which flow throughout the system. Land segments are *transformation resources*. River segments are *transportation resources*. Outlet points and estuaries are *independent buffers*. Buffers include both transformation resources and independent buffers. Thus, land segments, outlet points, and estuaries collectively form the set of *buffers*.

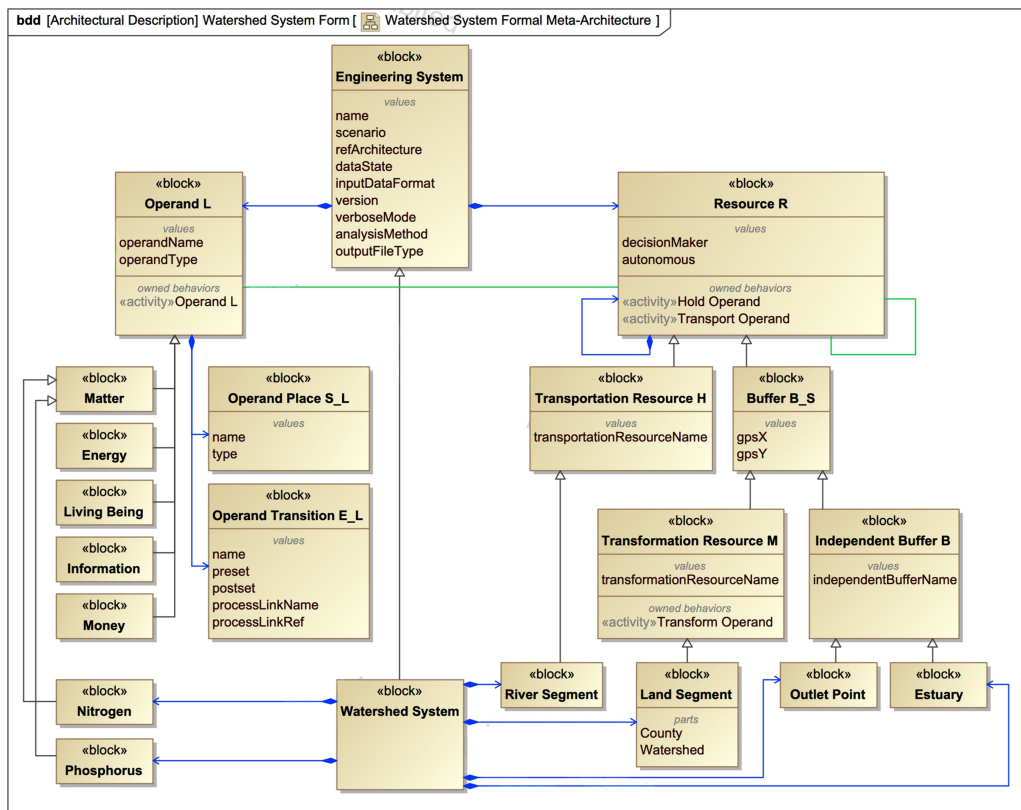


Figure 4: Block Definition Diagram of Watershed Systems

### 3.2. Activity Diagram of Watershed Systems

The processes enabled by these resources are shown in the watershed-specific ACT (Fig.5), which specializes the ACT defined by the engineering system meta-architecture (Fig.2). These processes transform and transport

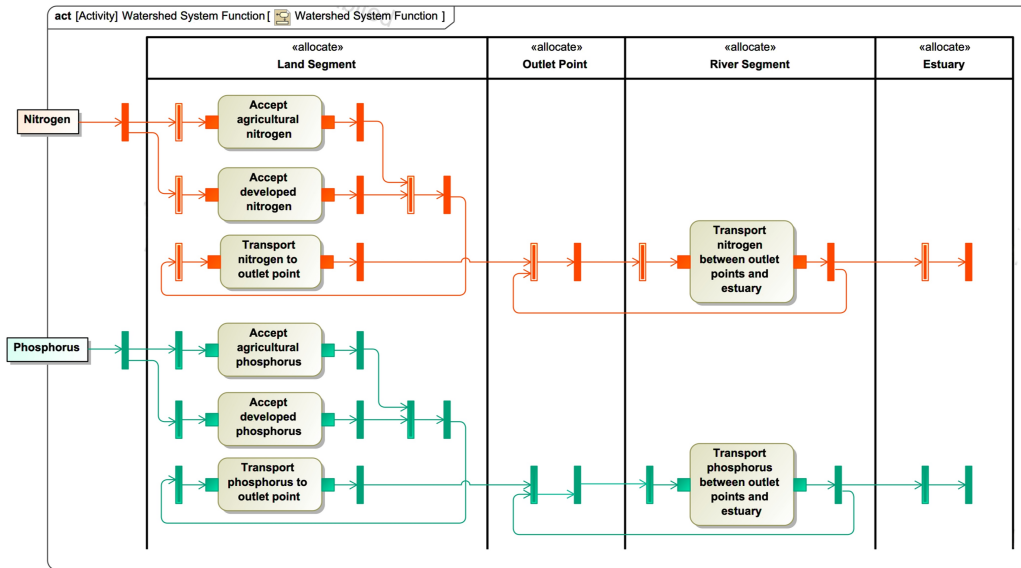


Figure 5: Activity Diagram of a Generic Watershed System

the system *operands*, nitrogen and phosphorus, as demonstrated in the HFGT meta-architecture formulation in Fig. 2. Each resource class has the following capabilities. Land segments can 1. accept agricultural nitrogen, 2. accept agricultural phosphorus, 3. accept developed nitrogen, 4. accept developed phosphorus, 5. transport nitrogen from the land segment to its outlet point, and 6. transport phosphorus from the land segment to its outlet point, where agricultural and developed nutrients refer to the sector applying the nutrient to the land. River segments can 1. transport nitrogen from outlet point to outlet point or to the estuary and 2. transport phosphorus from outlet point to outlet point or to the estuary. The formulation enforces explicit conservation of nutrient mass. Any nutrients not delivered to the estuary remain stored in upstream buffers, including land segments and outlet points. In this representation, buffer storage represents all retained nutrient mass, aggregating both physical accumulation and any unmodeled losses within the watershed. In the ACT (Fig. 5), these dynamics appear as the vertical joins and forks linking operand flows within each buffer class: land segment, outlet point, and estuary. In such a way, this model infers how nitrogen and phosphorus that are applied upstream are released at downstream locations in the watershed.

### 3.3. HFGT Definitions

With the RA for the generic watershed system defined, the watershed system is classified by the HFGT definitions introduced in Subsection 2.2. These terms form the following sets and indices, adopting the tensor-based notation of HFGT introduced in Farid et al. [72]:

**Operands**  $l_i \in L$  (**Defn. 3**): In this watershed system,  $L = \{N, P\}$ . Notably, water is not included amongst the system's operands because the CAST software does not track water flows. This modeling demonstrates how the WLSHFGSE is not just applicable to different systems but can also be tailored to accommodate simplifying modeling assumptions about those systems.

**Processes**  $p_w \in P$  (**Defn. 4**): represent actions operating on operands. As shown in Fig. 5, these include transformation processes that accept agricultural nitrogen, developed nitrogen, agricultural phosphorus, and developed phosphorus on land segments and transportation processes that move the nitrogen and phosphorus from land segments to outlet points, to river segments. As shown in Fig. 5, these processes are realized by land segments and river segments.

**Resources**  $r_v \in R$  (**Defn. 5**):.

- Each land segment is a transformation resource  $m \in M \subset R$ . The boundaries of each land segment are defined by a polygon formed by the intersection of a county and a river segment.
- Each river segment is a transportation resource  $h \in H \subset R$ .
- Each outlet point or estuary is an independent buffer  $b \in B \subset R$ .

**Buffers**  $b_{sy} \in B_S = M \cup B$  (**Defn. 6**): include land segments, outlet points and estuaries.

**Capabilities**  $\epsilon_\psi \in \mathcal{E}_f$  (**Defn. 7**): Fig. 5 shows 8 types of capabilities:

- Land segment accepts agricultural nitrogen.
- Land segment developed nitrogen.
- Land segment transports nitrogen to outlet point.
- Land segment accepts agricultural phosphorus.

- Land segment developed phosphorus.
- Land segment transports phosphorus to outlet point.
- River segment transports nitrogen between outlet points and estuary.
- River segment transports phosphorus between outlet points and estuary.

These are instantiated with each instantiated resource in the watershed.

#### 4. Application of WLSEHFGSE to Watershed Systems

Once the HFGT Meta-architecture and its constituent definitions have been applied to watershed systems, this section proceeds to apply the generic WLSEHFGSE first introduced in Subsection 2.3. This model estimates operand flows over time incorporating observed data from specific watershed, land use and economic systems while preserving physical and structural constraints. Importantly, the WLSEHFGSE is stated generically, enabling its application to a variety of complex systems of systems. Specific systems, however, place limiting conditions on this general form. When the general form of the WLSEHFGSE in Eq. 7 incorporates the physical characteristics of watershed systems, it collapses to the following specialized form:

$$\min Z = \sum_{k=1}^{K-1} [(\mathcal{E}_U^T[k]F_{\mathcal{E}}\mathcal{E}_U[k]) + (U^T[k]A_U U[k]) + (Q_B[k]^T A_{Q_B} Q_B[k])] \quad (14a)$$

subject to:

$$-Q_B[k+1] + Q_B[k] + (M^+ - M^-)U[k]\Delta T = 0 \quad \forall k \in \{1, \dots, K\} \quad (14b)$$

$$D_U U[k] - C_U[k] = \mathcal{E}_U[k] \quad \forall k \in \{1, \dots, K\} \quad (14c)$$

$$Q_B[1] = 0 \quad (14d)$$

where the decision variables are reduced to

$$x[k] = [Q_B; U; \mathcal{E}_U][k] \quad \forall k \in \{1, \dots, K\} \quad (14e)$$

to account for buffer stocks of each operand  $Q_B[k]$ , the flows of operands through capabilities  $U[k]$ , and the measurement error  $\mathcal{E}_U[k]$  associated with exogenous data  $C_U[k]$ .

#### 4.1. Derivation of the Specialization

The watershed-specific form of the WLSEHFGSE stated in Eq. 14 is derived from the general form in Eq. 7 by incorporating the following physical characteristics of watershed systems.

- The objective function in Eq. 7a simplifies to Eq. 14a when
  - only the dependence on the decision variables in Eq. 14e is included, and the linear terms are eliminated.
  - The time-invariant, diagonal, quadratic coefficient matrix  $F_{\mathcal{E}}$  imposes a weight on the square of each measurement error. This is expressed as in  $\mathcal{E}_U^T[k]F_{\mathcal{E}}\mathcal{E}[k]$  in matrix algebra.
  - The time-invariant, diagonal, quadratic coefficient matrices  $A_U$  and  $A_{Q_B}$  impose small quadratic penalties to flows and buffers. Values of  $\alpha = 10^{-10}$  and  $\beta = 10^{-12}$  are used for each of the diagonal terms in each of the matrices, respectively. Mathematically, these penalty terms help the optimization solver identify a single, stable solution.
- $k_{d\psi} = 0 \forall k \in \{1, \dots, K\}, \forall \psi \in \{1, \dots, \mathcal{E}_S\}$ : This RA assumes data inputs for all capabilities represent annual totals that occur instantaneously within the temporal resolution of the chosen annual time step. As a result,
  - Equation 7b simplifies to 14b to describe the mass balance of nitrogen and phosphorus throughout the watershed. Nutrient tracking requires explicit buffer stocks,  $Q_B$ . Each land segment, outlet, and the estuary is represented as a buffer with its own mass balance.
  - Equation 7c simplifies to  $Q_{\mathcal{E}}[k+1] - Q_{\mathcal{E}}[k] = 0 \forall k \in 1, \dots, K$  and can therefore be removed.
  - Eq. 7d simplifies to  $U^+[k] = U^-[k] = U[k]$  and can therefore be removed. A new variable,  $U[k]$  is introduced to simplify notation.
  - Eq. 7j simplifies to 14c to describe the exogenously defined firing vector weights, or flows, of the watershed system.

- $S_{l_i} = 0 \forall l_i \in L$ : This watershed system assumes that the state of nitrogen and phosphorus do not change. All nitrogen and phosphorus are counted as total mass inclusive of all chemical formulations. Therefore, there are no operand nets that track the state of these operands. As a result, Eqs. 7e-7i and 7k are removed.
- Eq. 7l simplifies to 14d, setting the initial value of accumulated nutrients to zero at the beginning of the simulation.
- For Eq. 7n, the absence of data constraining the upper and lower bounds of nutrient flows means that this constraint can be removed.
- For Eq. 7o, the CAST software does not include effort variables  $Y$  (e.g., nutrient concentrations) because it does not track water flows. Consequently, this constraint can be removed as well.

#### 4.2. Weighted Least Squares Error Objective Function

The objective function of the watershed system takes the form described in Eq. 14a, minimizing the weighted sum of squared errors on the exogenously defined flows  $C_U$ . This paper assumes that all data utilized to exogenously define the firing vectors have equal magnitude of percent error in the absence of evidence to the contrary. However, because the resulting flows have different characteristic magnitudes, their error terms can have a disproportionate impact on the objective function. This study adopts the weighting strategy used in the AMES implementation of the WLSEHFGSE [13] which normalizes each error term for the exogenous constant calculated for the flow.

$$F_{\mathcal{E}} = \text{diag} \left( \frac{1}{\max(C_U^2, 2)} \right) \quad (15)$$

#### 4.3. Watershed Engineering System Net State Transition Function

The state transition function (Eq. 14b) retains the full continuity equation with incidence matrix  $M^{\pm}$ . The incidence tensor in matrix form represents extraction of each nutrient-operand from buffers by capabilities and their injection back into new buffers. Subsection 5.1 outlines the construction of the hetero-functional incidence tensors for the instantiated CBW system.

#### 4.4. *Watershed Engineering System Net Measurement Function*

The measurement of exogenously defined variables is largely dependent on the instantiated system. Subsection 5.2 outlines the development of exogenously defined flows for the instantiated CBW.

#### 4.5. *Initial Conditions*

The initial conditions constraint (Eq. 14d) defines the initial stock of nutrients in each buffer to be zero. Thus, the value of  $Q_B$  represents the accumulation of nutrients beginning from the start to the end of the simulation from time step  $\{1, \dots, K\}$ .

### 5. **Application of the Watershed Specific WLSEHFGSE to the Chesapeake Bay Watershed System**

This section describes the practical implementation of the water-specific HFGT–MBSE framework introduced in Sections 3 and 4. Subsection 5.1 details the synthesis of the hetero-functional incidence matrix used to construct the Watershed Engineering System Net State Transition Function (Eq.14b, Subsection4.3). Subsection 5.2 then explains how CAST source and scenario data inform the watershed engineering system net measurement function (Eq.14c, Subsection4.4).

#### 5.1. *Processing CAST Geospatial Data for the Engineering System Net State Transition Function*

The synthesis of the hetero-functional incidence tensor for the watershed engineering system net state transition function (Eq.14b) begins with constructing a spatially explicit formal representation of the CBW. The purpose of this geospatial workflow is to generate the GIS-based resource definitions needed for the HFGT toolbox input file and, ultimately, the hetero-functional incidence matrix that encodes which capabilities inject or eject each operand for every CAST-defined buffer (e.g., “Land Segment X, nitrogen” or “Outlet Y, phosphorus”). These resources and capabilities follow directly from the watershed-specific BDD (Fig.4) and its associated activity diagram (Fig. 5).

A spatially explicit model of the CBW was developed to reconstruct the implicit routing logic of CAST using publicly available geospatial data (Fig. 6). This representation defines how flows move from land–river segments through the stream network to the estuary, providing the structural

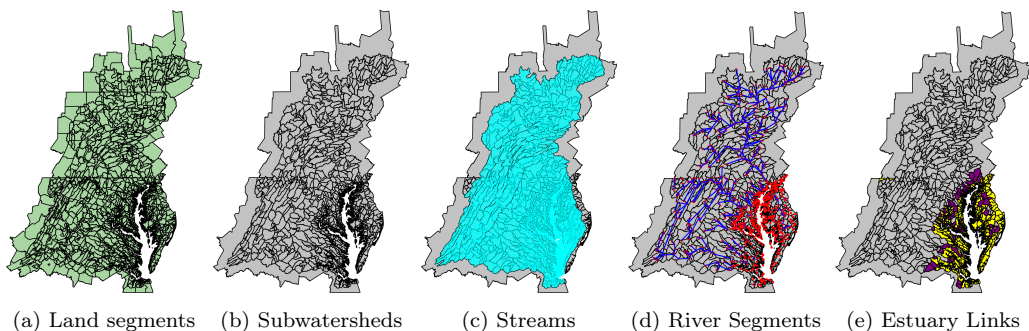


Figure 6: Derivation of a formal representation of the Chesapeake Bay Watershed

foundation necessary for integrating watershed systems into the HFGT framework.

The workflow begins with CAST land–river segment polygons (Fig.6a). These polygons are merged by shared subwatershed boundaries to generate river-segment polygons (Fig.6b). A 30-m digital elevation model (DEM) is then used to perform a flow-accumulation analysis. For each segment, the point of maximum accumulated flow is extracted and designated as a provisional outlet. This provides an initial estimate of where water exits that subwatershed.

These provisional outlets are compared with the locations where CAST stream lines intersect each polygon (Fig. 6c). Segment boundaries are converted to lines and intersected with the stream network, producing a dense set of candidate crossing points. Because the CAST stream dataset includes streams of multiple orders, there are substantially more intersection points than subwatersheds.

To determine the final outlet for each segment, provisional outlets are snapped to the most appropriate intersection point. Terminal segments are snapped to intersections on the estuary boundary, whereas internal segments are snapped to intersections consistent with downstream neighbors. This step aligns the spatial model with CAST naming conventions including trailing identifiers (e.g., “0000” for estuarine segments, “0001” for directly upstream segments).

After finalizing outlet locations, directed flowlines are constructed between upstream and downstream outlets (Fig.6d). These relationships are inferred from the CAST segment naming structure, which encodes upstream and downstream connectivity. Segments draining directly to the estuary are

linked to the nearest estuarine boundary (Fig.6e). Spatial attributes are then harmonized. Segment identifiers and labels are updated for consistency. Centroids are then computed for visualization and aggregation, and outlet points are annotated with coordinates and flow direction metadata. Together, these operations produce a coherent and reproducible graph of watershed connectivity across the entire CBW.

With the geospatial representation complete, the resulting shapefiles are used to construct the HFGT toolbox input file that defines each resource type, operand, and capability according to the watershed RA (Fig. 4 and Fig. 5). For each buffer–operand pair (e.g., “Land Segment X, nitrogen”), the toolbox records which capabilities inject or eject each operand, as specified by the watershed activity diagram (Fig. 5). These relationships populate the hetero-functional incidence matrix,  $M$ , a core structural component of the HFGT formulation. This matrix, derived directly from the geospatial reconstruction, provides the structural basis for the watershed engineering system net state transition function used in the WLSEHFGSE formulation.

### 5.2. Processing CAST Behavioral Data for the Measurement Function

Complementing the formulation of the hetero-functional incidence matrix described in the previous subsection, CAST behavioral data is used to derive the watershed engineering system net measurement function. Equation 14c imposes exogenous measurements on the firing vector  $U$ . In this equation,  $D_U$  is a selection matrix that maps CAST-provided measurements to the corresponding capabilities in  $U$ . Its dimensions are given by the number of measurement values in  $C_U[k]$  (rows) and the total number of capabilities represented in  $U$  (columns). The vector  $C_U[k]$  contains constant estimates of operand flows at each time step, derived directly from CAST datasets (Table 1), with each entry corresponding to an empirical value for a specific class of watershed system process or resource.

It is important to note that the WLSEHFGSE formulation supports the incorporation of data that is coarse or incomplete both temporally and spatially [13]. In place of a single selection matrix  $D_U$ , separate capability and temporal aggregation matrices— $D_{\mathcal{E}}$  (Defn.14) and  $D_T$  (Defn.15) respectively—can be used to aggregate firing-vector data across capabilities and time steps. These matrices can be synthesized systematically using matrix algebra. In the present instantiation of the CBW system, which involves a single time step, the temporal aggregation matrix reduces to the identity matrix.

**Definition 14 – Capability Aggregation Matrix  $D_{\mathcal{E}}$  [13]:** The capability aggregation matrix  $D_{\mathcal{E}} \in \{0, 1\}^{|\mathcal{E}_S| \times |\mathcal{E}_D|}$  is a matrix whose element  $D_{\mathcal{E}}(\psi_1, \psi_2) = 1$  when the flow associated with system capability  $\epsilon_{\psi_2} \in \mathcal{E}_S$  is part of the flow associated with data element  $\tilde{C}_U(\psi_1, k)$  at time  $k$ . ■

**Definition 15 – Temporal Aggregation Matrix  $D_T$  [13]:** The temporal aggregation matrix  $D_T \in \{0, 1\}^{K \times K_D}$  is a matrix whose element  $D_T(k_1, k_2) = 1$  when the flows associated with time step  $k_1 \in \{1, \dots, K\}$  corresponds to the flows associated with  $k_2 \in \{1, \dots, K_D\}$  in the data  $\tilde{C}_U$ . ■

Furthermore, this implementation represents a preliminary instantiation of the Chesapeake Bay Watershed system modeling suite within the HFGT meta-architecture, using CAST data to exogenously define all known flows within the watershed domain. While this formulation captures the major nutrient pathways represented in CAST, the structure of the model readily accommodates the inclusion of additional variables and data sources. Many other quantities available within CAST, such as BMP efficiencies or atmospheric and point-source loadings, can be incorporated as additional constraints on exogenous flows. As the CBP continues to expand its data and model resolution, new datasets can be integrated directly into the HFGT framework, enabling improved fit and enhanced representation of the dynamic system.

Table 1 summarizes the exogenous data sets from CAST that inform the engineering system net measurement function in the WLSEHFGSE formulation. Each row corresponds to a specific subset of engineering-system capabilities that inform particular entries of the system’s net firing vector  $U$  and identifies the empirical quantities against which those flows are constrained. In this way, the table establishes the direct mapping between CAST’s reported physical measurements and the capability-level equality constraints imposed in the state estimator.

**Accept (agricultural/developed) (nitrogen/phosphorus).** The *Nutrients Applied* dataset provides the empirical measurements for all accept processes ( $p = 0-3$ ) that introduce nitrogen and phosphorus into land buffers. These values correspond directly to the elements in  $U[k]$  associated with agricultural and developed applications across all land segments in each county. For every county and sector, the CAST-reported total applied nitrogen or phosphorus must equal the sum of the corresponding accept firings in  $U$  and error term  $\mathcal{E}_U$ , ensuring consistency between system inputs and CAST’s sector-level nutrient applications.

Table 1: Exogenous datasets used in the CAST WLSEHFGSE model. All data is obtained from the Chesapeake Assessment Scenario Tool (CAST Version 2023, Phase 6).

Corresponding		Dataset	Date	Granularity		Extracted Data
Processes	Resources			Temporal	Spatial	
Accept (ag. <sup>a</sup> /dev. <sup>b</sup> ) (N <sup>c</sup> /P <sup>d</sup> )	Land segments	Nutrients Applied	2024	Annual	County	Total applied (N/P) by sector
Transport (N/P)	Land & river segments	Loads Report	2024	Annual	County	EoS & EoT
Transport (N/P)	Land & river segments	Base Conditions Report	2024	Single base year	Land-river segment	Load source area
Transport (N/P)	Land & river segments	Source Data Report	–	Steady state	Land-river segment	Delivery factors by load source

<sup>a</sup>nitrogen, <sup>b</sup>phosphorus, <sup>c</sup>agricultural, <sup>d</sup>developed

**Transport (nitrogen/phosphorus).** Estimating the net firing values associated with transport processes requires data drawn from three CAST sources: the *Loads Report*, the *Base Conditions Report*, and the *Source Data Report*. Each provides a complementary component of the measurement function used to constrain the corresponding set of transport capabilities.

EoS values from the *Loads Report* constrain the aggregated transport of nutrients from land segments to their associated outlet points. In the HFGT representation, these quantities correspond to entries of  $U[k]$  for land-to-stream transport capabilities. For each county, the total EoS load must match the sum of the appropriate transport-process firings across all land segments within the county including the corresponding error term  $\mathcal{E}_U$ .

EoT values, also reported in the *Loads Report*, specify the total amount of nitrogen and phosphorus delivered to the estuary. Because the HFGT network removes CAST’s direct land-to-estuary mapping in favor of explicit downstream routing, these data constrain all capabilities whose destination buffer is the estuary. Accordingly, the sum of all outlet-to-estuary transport firings in  $U[k]$  and the corresponding error terms  $\mathcal{E}_U$  is set equal to the CAST-reported EoT totals.

The *Base Conditions Report* provides load-source areas for each land-river segment, allowing the computation of weighted averages of load-source-

dependent delivery factors. These weights ensure that delivery factors extracted from CAST are assigned to the correct resource and its associated capability.

The *Source Data Report* supplies delivery factors governing attenuation across CAST’s three transport stages: land-to-water, stream-to-river, and river-to-bay. For each land segment, delivery factors for different load-source types were aggregated using load-source areas from the *Base Conditions Report* to form a single weighted delivery factor. For land-to-stream transport, the relevant entries of  $U[k]$  and  $\mathcal{E}_U$  depend on the inflow to a land segment multiplied by delivery factors  $DF_{\text{land}\rightarrow\text{water}}$  and  $DF_{\text{stream}\rightarrow\text{river}}$ .

For transport between outlet points, delivery factors require an additional derivation: dividing the upstream and downstream river-to-bay delivery factors yields the fraction of flow routed between consecutive outlet points. These derived factors become the coefficients linking inflow expressions to their associated firing values  $U[k]$  and  $\mathcal{E}_U$  for stream-network transport processes.

Because outlet points are defined on river segments and multiple land segments may map to a single segment, delivery factors for each outlet buffer are averaged across all contributing land segments. This ensures that every transport capability, whether land-to-outlet, outlet-to-outlet, or outlet-to-estuary, is grounded in CAST’s empirical attenuation structure and enters the watershed engineering system net measurement function through clearly defined entries of the net firing vector  $U[k]$ .

## 6. Visualized Results & Discussion

### 6.1. Results

For this analysis, the reconstructed HFGT-based watershed model was executed for the “2024 Progress” scenario [25] as a single, steady-state time step of the CAST model. While the framework is capable of representing multiple temporal scenarios as a dynamic simulation, this study focuses on model development and verification. The selected run illustrates how the MBSE-HFGT formulation reproduces CAST’s validated watershed-scale loading patterns while providing a first-pass, reconstruction of internal river network connectivity using CAST-derived, primarily regression-based, behavioral data. This initial reconstruction is intended to identify where available data strongly constrain flows and where uncertainty is dominated by sparsity or aggregation, motivating future work on measurement-error

weighting. Figures 7-9 and Table 2 summarize the reconstructed nitrogen and phosphorus dynamics.

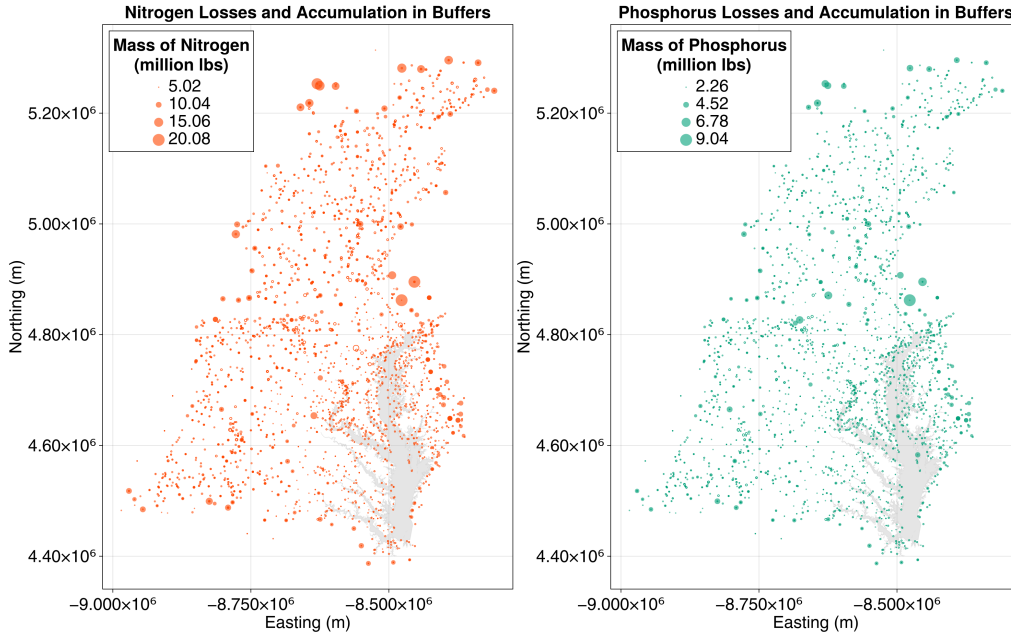


Figure 7: Accumulation of nitrogen and phosphorus in the Chesapeake Bay Watershed within land segments and outlet points

The spatial distribution of accumulated nitrogen and phosphorus masses (Fig. 7) demonstrates that nutrient retention and delivery are highly heterogeneous across the CBW. While CAST provides total delivered loads per land-river segment, the HFGT formulation explicitly traces the routing of these masses through connected outlet points, making visible the cascading transport of nutrient loads from upstream subwatersheds to the estuary. This spatially distributed mass enables the identification of critical intermediate nodes—points along the river network—that disproportionately accumulate and transport nutrients. The CBP has acknowledged a related limitation of CAST: although mass is conserved in aggregate, the segment-level delivery factors represent losses and accumulation in a lumped manner, obscuring how mass balance is distributed across the river network [15].

Further, Fig. 8 disaggregates the relative contribution of economic sectors to applied nutrient loads within land segments. Combined with the flow reconstruction, this allows for sector-specific tracing of nutrient delivery path-

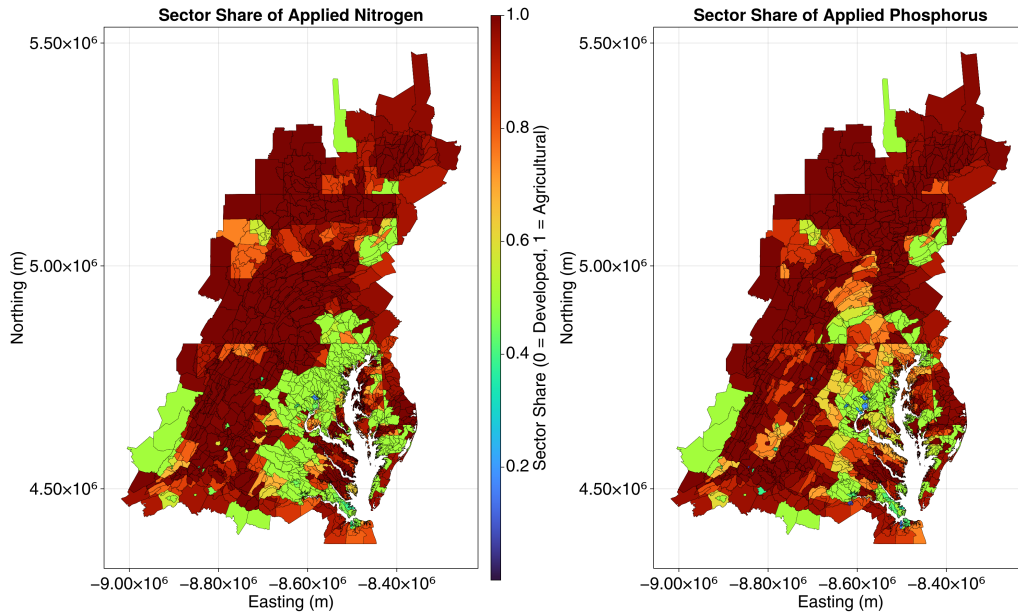


Figure 8: Economic sector relative contribution to applied nitrogen and phosphorus on land segments

ways. While CAST provides sector-level nutrient inputs as static scenario data, incorporating these data within the MBSE-HFGT framework transforms them into functional elements of an interconnected network model, enabling explicit integration with economic and policy systems and facilitating future coupling with domain-specific models.

Finally, the reconstructed transport network (Fig. 9) visualizes nutrient movement through delineated river segments, revealing the implicit topological structure underlying the aggregated delivery factors of CAST. In the original CAST model, nutrient attenuation is represented as a single empirical coefficient mapping the load of each land-river segment directly to the estuary. In contrast, the HFGT network decomposes this aggregate relationship into sequential flows between subwatersheds connected in a river network, conserving mass at each node and quantifying intermediate fluxes between neighboring outlets. This transformation enables structural analysis and creates a pathway to dynamic simulation by expressing CAST's aggregate delivery relationships as an explicit sequence of network flows and intermediate states.

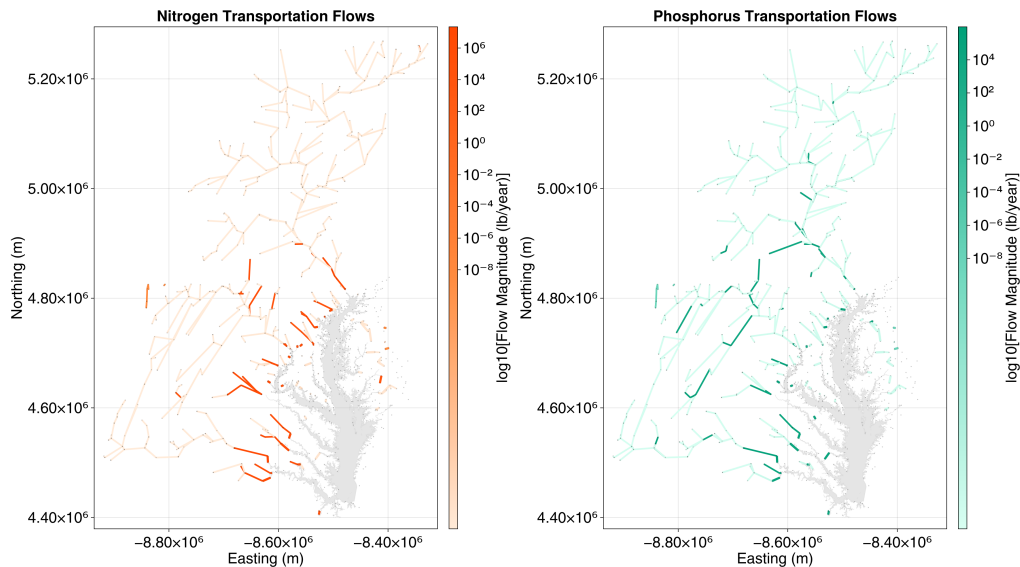


Figure 9: Flow of nitrogen and phosphorus through delineated river segments in the Chesapeake Bay Watershed

These reconstructed transport magnitudes span approximately 14 orders of magnitude ( $10^{-8}$  to  $10^6$  lbs), necessitating logarithmic visualization to simultaneously resolve both small tributary inputs and large mainstem flows. This extreme range reflects the hierarchical nature of watershed hydrology: headwater segments drain small catchments with minimal cumulative loads, while downstream confluences integrate contributions from progressively larger drainage areas. The largest flows, those entering the estuary, represent the cumulative nutrient transport from the entire watershed, whereas the smallest flows correspond to localized land-to-stream transfers in sparsely developed or low-intensity agricultural subwatersheds. This magnitude of heterogeneity reflects an inherent characteristic of dendritic river networks, in which flow accumulation follows a power-law relationship with drainage area [73]. The logarithmic scale ensures that both ecologically significant headwater processes, which govern local water quality and in-stream retention, and system-level mass balances, which determine estuarine nutrient loading, remain visible within a single spatial representation.

To assess the performance of the model, Table 2 summarizes the goodness of fit relative to CAST-published nutrient loads. The HFGT reconstruction captures the major spatial patterns present in CAST’s empirical data while

Table 2: Summary of model fit and estimation error across data types for nitrogen and phosphorus.  $R^2$  and NRMSE are computed relative to the data in Table 1.

<b>Data Type</b>	<b>Dataset</b>	<b>Metric</b>	<b>N</b>	<b>P</b>
<i>Total applied by county and sector</i>	Nutrients	$R^2$	0.910	0.842
	Applied	NRMSE	57.6%	86.6%
<i>EoS</i>	Loads Report	$R^2$	0.290	-0.0720
		NRMSE	107%	111%
<i>EoT</i>	Loads Report	Relative Error	< 0.01%	< 0.01%
<i>Stream to Tide</i>	Loads Report	Relative Error	8.86%	28.3%
<i>Transportation</i>	Source Data & Base Conditions Reports	Relative Error (median)	34.0%	

also exhibiting expected deviations that arise from replacing CAST’s aggregate regressions with an explicitly structured mass-transport network.

Within the county-level constraints, applied nutrient inputs were aggregated for each county and sector and enforced as equality conditions between CAST-reported applications and the corresponding accept capabilities. These constraints ensure that all nutrient mass entering the modeled system are consistent with CAST’s sector-level inputs. As shown in Table 2, applied nitrogen and phosphorus exhibit moderately strong correspondence with CAST values ( $R^2 = 0.91$  and  $0.84$ , respectively), although the normalized RMSE remains high (58–87%). These larger relative errors reflect spatial heterogeneity in CAST’s land-segment-level application data, which is also reported by load source and is partially homogenized when aggregated to county-by-sector constraints in the WLSEHFGSE formulation.

Similarly, EoS loads—computed in CAST as land-to-outlet point deliveries—were compared directly against the land to outlet transport capabilities aggregated by county in the HFGT network. Agreement at the EoS scale is lower than at the watershed aggregate (Table 2), which is expected in this first-pass reconstruction. Namely, EoS values reflect CAST-derived, regression-based delivery behavior. Importantly, the result is diagnostic rather than problematic. Under the present formulation, constraints are uniformly weighted, so EoS equations do not dominate the solution relative to the much larger set of transport-consistency relationships they describe. This directly motivates a next-step WLSEHFGSE formulation in

which measurement-error weights reflect data provenance and reliability (e.g., EoS vs. transport consistency vs. aggregated totals), allowing the estimator to prioritize fitting decision variables that are data-rich.

At the aggregated Chesapeake Bay Watershed (CBW) scale, the model achieves nearly exact agreement with CAST-reported EoT totals for both nutrients ( $< 0.01\%$  error; Table 2). This near-perfect closure demonstrates that the reconstructed HFGT network preserves system-level mass balance despite local deviations. Likewise, the WLSEHFGSE estimator correctly routes the total nutrient load through the dendritic hydrologic network. Stream-to-Tide (outlet-to-outlet) aggregates exhibit higher discrepancies (9% for N and 28% for P), reflecting differences between CAST’s lumped delivery factors and the explicit river network routing represented in the HFGT model. These deviations again highlight the consequences of uniformly weighting all constraint equations: system-level flows, though conceptually central, are not preferentially emphasized in the optimization and thus may deviate from CAST targets, a key insight for prioritizing additional data and refining weighting.

The transport-capability residuals are largest where CAST behavioral information is most aggregated and least directly observed, i.e., where regression-based delivery factors are being translated into reach-resolved routing. This is an expected outcome of moving from a lumped statistical representation to an explicit network: the reconstruction reveals where intermediate fluxes are weakly identifiable given currently available data, and therefore where future measurement campaigns or differentiated weighting would provide the greatest benefit.

Three methodological factors explain these deviations. First, CAST specifies nutrient delivery as single empirical coefficients mapping each land–river segment directly to the estuary, whereas the HFGT reconstruction decomposes these aggregate coefficients into sequential outlet-to-outlet flows. This decomposition exposes variability that CAST’s formulation implicitly averages. Second, CAST delivery factors were spatially downscaled from the land-river segment level for outlet-to-outlet transportation capabilities and assigned to river segments. This produced localized mismatches between land-river segment level coefficients. Third, CAST assigns delivery factors by land-use-dependent load source, whereas the HFGT reconstruction models in-stream delivery uniformly across upstream nutrient sources. This distinction is physically informed: in-stream attenuation processes (e.g., denitrification, sedimentation) do not retain memory of land-use origin once nutrients enter the stream network. However, because CAST’s delivery factors are

statistically associated with originating land-segment attributes, applying uniform in-stream propagation changes the statistical target being matched locally, which is expected to increase local discrepancies while improving physical interpretability for analysis of the full river network.

Across all constraint types, these deviations represent the expected outcome of transforming CAST’s multiscale, regression-based framework into an explicit physical network model. Crucially, the aggregate mass-balance closure (errors  $< 0.01\%$  at EoT) demonstrates that these local deviations offset rather than accumulate. This behavior aligns with well-established findings in spatially distributed hydrologic modeling, where parameter uncertainty and local discrepancies tend to diminish at broader spatial scales [74, 75]. More importantly, the results underscore that a future WLSE-HFGSE formulation should incorporate a principled weighting scheme that reflects the differing reliability, scale, and interpretive importance of EoS, EoT, and transport constraints, rather than treating all capability equations as equally informative in the optimization.

## 6.2. Discussion

Overall, the HFGT-based formulation preserves the empirical accuracy of CAST at the watershed scale while fundamentally expanding its structural and behavioral interpretability. By reconstructing the implicit flow network underlying the aggregated delivery factors of CAST, the model exposes the internal pathways of nutrient transport and quantifies accumulation across nested subwatersheds. Likewise, the model links economic-sector nutrient applications within the new, explicit network. Where CAST provides validated estimates of nutrient loading to the estuary, the HFGT reconstruction reveals how those loads distribute across the watershed.

This shift from a statistical to a physically structured formulation represents a deliberate design emphasis: this first-pass reconstruction preserves CAST’s watershed-scale empirical behavior while prioritizing structural transparency and extensibility at intermediate scales. Local discrepancies are informative because they indicate where CAST-derived behavioral data are insufficient to uniquely determine intermediate fluxes, guiding both future data collection and principled weighting of measurement error. The explicit representation of transport pathways allows the model to serve as a foundation for new analytical capabilities not possible within the existing CAST framework. These include dynamic simulation of temporal variability and assimilation of monitoring data for real-time state estimation. Achieving the full potential

of this framework, however, depends on the continued expansion and refinement of empirical data inputs. In particular, the CBP identified the need for new field-scale measurements to better quantify hydrologic and biogeochemical processes that drive nutrient attenuation and transformation across heterogeneous landscapes [15, 76, 77]. Incorporating such high-resolution field data, along with further CAST variables and datasets, will enable future model iterations to strengthen local parameterization. By bridging the empirical accuracy of CAST with mechanistic understanding, the HFGT-based approach provides a complementary tool for watershed analysis that utilizes existing modeling tools to gain new insights for stakeholders.

## 7. Conclusion & Future Work

This study develops an HFGT-based structural reconstruction of a real-world watershed system, demonstrating how MBSE and HFGT can formalize the physical and functional structure underlying an existing empirical model. The resulting framework reproduces the validated nutrient load estimates of the Chesapeake Bay Watershed case study model, CAST, while revealing previously hidden internal connectivity across the watershed. By explicitly representing the topological routing of flows between land, river, and estuary segments, the model transforms CAST from a static, aggregate assessment tool into a physically structured network capable of supporting system-of-system analysis.

Critically, this study represents a first-pass incorporation of the CAST behavioral datasets, many of which are regression-derived, into a unified state-estimation framework. The resulting residual patterns provide actionable guidance for future work in the region and future watershed system instantiations: they indicate which data types should carry higher weight, where constraints are currently under-informative, and which behaviors in the model are most sensitive to sparse or highly aggregated measurements. The HFGT formulation establishes an extensible foundation for integrating additional processes and domains that influence watershed function.

Future work towards the Chesapeake Bay Watershed case study can focus on coupling this model to the estuary model by incorporating freshwater delivery and nutrient phase partitioning (particulate versus dissolved) to improve representation of land–estuary connectivity [78]. Similarly, assimilating monitoring data to estimate intermediate fluxes and refine spatial variability in nutrient transport would enhance accuracy of constructed

flows [30, 41]. These efforts would benefit from ongoing collection of high-resolution, field-scale measurements of hydrologic and biogeochemical processes [79, 76, 77]. Finally, because CAST is a time-averaged statistical emulator of the original HSPF-based watershed model, a natural next step is to compare the reconstructed HFGT network against outputs from the fully dynamic HSPF lineage to evaluate consistency in spatial routing and mass conservation [16, 32]. Beyond the watershed system, the extensibility of the MBSE-HFGT architecture enables integration with models of human systems that shape nutrient dynamics. Economic models can represent sector-level decision-making, costs, and incentives associated with nutrient management practices, while governance models can capture institutional and regulatory feedbacks influencing implementation across jurisdictions. Embedding these social, economic, and policy processes within a shared framework will enable multi-domain scenario evaluation.

However, the primary contribution of this work lies in demonstrating the method through a case study, which establishes a basis for future extension to additional watershed and environmental systems. This paper demonstrates that coupling MBSE and HFGT provides a sound pathway for extending large-scale watershed and environmental models, such as CAST, into system of systems modeling frameworks without sacrificing empirical accuracy or mechanistic structure. Further, the approach supports dynamic simulation and adaptive management across environmental, economic, and governance domains. The HFGT-based model thus serves not as a replacement for regional models such as CAST, but as their structural complement, one that renders the complex socio-environmental dynamics of the large-scale watershed systems of systems in an explicit manner for future interdisciplinary research.

## **Acknowledgments**

This research is based on work supported by the Growing Convergence Research Program of the National Science Foundation under Grant Numbers OIA 2317874 and OIA 2317877.

## **Data and Code Availability**

The modeling framework presented in this study was implemented using the Hetero-functional Graph Theory (HFGT) toolbox and custom Python

and Julia scripts developed by the authors. The code required to reproduce the simulation results is publicly available in a version-controlled GitHub repository at <https://github.com/LIINES/HFGT-CBW-Watershed-Model>.

The data associated with the Chesapeake Bay watershed simulation, along with detailed instructions for constructing the required directory structure, are archived on Zenodo at <https://doi.org/10.5281/zenodo.18763339>.

This study uses publicly available data products from the Chesapeake Assessment Scenario Tool (CAST), developed by the Chesapeake Bay Program [25], together with associated Chesapeake Bay Program geospatial datasets [27]. All model inputs were derived from these public sources through documented preprocessing and aggregation steps.

No proprietary or restricted datasets were used in this study. Reproduction of the results requires only a standard personal computer and the open-source software listed in the repository.

## CRediT Author Statement

**Megan S. Harris:** Conceptualization, Methodology, Software, Validation, Formal analysis, Investigation, Writing - Original Draft, Visualization, Project Administration. **Dr. John C. Little:** Conceptualization, Resources, Writing - Review & Editing, Supervision, Project Administration, Funding Acquisition. **Dr. Amro M. Farid:** Conceptualization, Methodology, Software, Validation, Writing - Review & Editing, Supervision, Project Administration, Funding Acquisition.

## References

- [1] C. Folke, S. Polasky, J. Rockström, V. Galaz, F. Westley, M. Lamont, M. Scheffer, H. Österblom, S. R. Carpenter, F. S. Chapin, et al., Our future in the anthropocene biosphere, *Ambio* 50 (2021) 834–869.
- [2] J. Rockström, Bounding the planetary future: Why we need a great transition, *Great Transition Initiative* (01 2015).
- [3] F. Biermann, X. Bai, N. Bondre, W. Broadgate, C.-T. Arthur Chen, O. P. Dube, J. W. Erisman, M. Glaser, S. van der Hel, M. C. Lemos, S. Seitzinger, K. C. Seto, Down to earth: Contextualizing the anthropocene, *Global Environmental Change* 39 (2016) 341–350.

doi:<https://doi.org/10.1016/j.gloenvcha.2015.11.004>.

URL <https://www.sciencedirect.com/science/article/pii/S0959378015300686>

- [4] F. Biermann, T. Hickmann, C.-A. Sénit, M. Beisheim, S. Bernstein, P. Chasek, L. Grob, R. E. Kim, L. J. Kotzé, M. Nilsson, et al., Scientific evidence on the political impact of the sustainable development goals, *Nature Sustainability* 5 (9) (2022) 795–800.
- [5] Ö. Bodin, Collaborative environmental governance: Achieving collective action in social-ecological systems, *Science* 357 (6352) (2017) ean1114. arXiv:<https://www.science.org/doi/pdf/10.1126/science.aan1114>, doi:10.1126/science.aan1114. URL <https://www.science.org/doi/abs/10.1126/science.aan1114>
- [6] M. S. Reed, Stakeholder participation for environmental management: A literature review, *Biological Conservation* 141 (10) (2008) 2417–2431. doi:<https://doi.org/10.1016/j.biocon.2008.07.014>. URL <https://www.sciencedirect.com/science/article/pii/S0006320708002693>
- [7] E. B. Daniel, J. V. Camp, E. J. LeBoeuf, J. R. Penrod, J. P. Dobbins, M. D. Abkowitz, Watershed modeling and its applications: A state-of-the-art review, *Open Hydrology Journal* 5 (1) (2011) 26–50.
- [8] S. Fatichi, E. R. Vivoni, F. L. Ogden, V. Y. Ivanov, B. Mirus, D. Gochis, C. W. Downer, M. Camporese, J. H. Davison, B. Ebel, N. Jones, J. Kim, G. Mascaro, R. Niswonger, P. Restrepo, R. Rigon, C. Shen, M. Sulis, D. Tarboton, An overview of current applications, challenges, and future trends in distributed process-based models in hydrology, *Journal of Hydrology* 537 (2016) 45–60. doi:<https://doi.org/10.1016/j.jhydrol.2016.03.026>. URL <https://www.sciencedirect.com/science/article/pii/S0022169416301317>
- [9] A. A. Keller, K. Garner, N. Rao, E. Knipping, J. Thomas, Hydrological models for climate-based assessments at the watershed scale: A critical review of existing hydrologic and water quality models, *Science of The Total Environment* 867 (2023) 161209.

doi:<https://doi.org/10.1016/j.scitotenv.2022.161209>.

URL <https://www.sciencedirect.com/science/article/pii/S0048969722083139>

- [10] SE Handbook Working Group, Systems Engineering Handbook: A Guide for System Life Cycle Processes and Activities, International Council on Systems Engineering (INCOSE), 2015.
- [11] ISO-IEC-IEEE, Systems and software engineering—system life cycle processes, ISO/IEC/IEEE Standard ISO/IEC/IEEE 21839:2019 (2019) 2008.
- [12] M. Harris, E. Ghorbanichemazkati, M. M. Naderi, J. C. Little, A. M. Farid, Demonstrating integrative, scalable modeling of hydrological systems with model-based systems engineering and hetero-functional graph theory (2025). arXiv:2506.00696.  
URL <https://arxiv.org/abs/2506.00696>
- [13] D. J. Thompson, A. M. Farid, A Weighted Least Squares Error Hetero-functional Graph State Estimator of the American Multi-modal Energy System, Submitted for Publication. Available at: URL pending (2025).
- [14] Chesapeake Bay Program, The estuary, <https://www.chesapeakebay.net/discover/ecosystem/the-estuary>, accessed [Month, Year]. (2020).
- [15] R. R. Hood, G. W. Shenk, R. L. Dixon, S. M. Smith, W. P. Ball, J. O. Bash, R. Batiuk, K. Boomer, D. C. Brady, C. Cerco, et al., The chesapeake bay program modeling system: Overview and recommendations for future development, *Ecological modelling* 456 (2021) 109635.
- [16] USEPA (U.S. Environmental Protection Agency), Chesapeake bay phase 5.3 community watershed model, Tech. Rep. EPA 903S10002 - CBP/TRS-303-10, U.S. Environmental Protection Agency, Chesapeake Bay Program Office, Annapolis, MD (December 2010).
- [17] Z. Easton, D. Scavia, R. Alexander, K. Boomer, P. Kleinman, A. Miller, J. Pizzuto, D. Smith, C. Welty, Scientific and technical advisory committee review of the chesapeake bay program phase 6 watershed model, *STAC Publ* (2017) 17–007.

- [18] J. D. Hagy, W. R. Boynton, C. W. Keefe, K. V. Wood, Hypoxia in chesapeake bay, 1950–2001: long-term change in relation to nutrient loading and river flow, *Estuaries* 27 (4) (2004) 634–658.
- [19] W. M. Kemp, W. R. Boynton, J. E. Adolf, D. F. Boesch, W. C. Boicourt, G. Brush, J. C. Cornwell, T. R. Fisher, P. M. Glibert, J. D. Hagy, et al., Eutrophication of chesapeake bay: historical trends and ecological interactions, *Marine ecology progress series* 303 (2005) 1–29.
- [20] M. R. Williams, S. Filoso, B. J. Longstaff, W. C. Dennison, Long-term trends of water quality and biotic metrics in chesapeake bay: 1986 to 2008, *Estuaries and Coasts* 33 (6) (2010) 1279–1299.
- [21] A. Buchheister, C. F. Bonzek, J. Gartland, R. J. Latour, Patterns and drivers of the demersal fish community of chesapeake bay, *Marine Ecology Progress Series* 481 (2013) 161–180.
- [22] J. H. Landsberg, S. Hall, J. N. Johannessen, K. D. White, S. M. Conrad, J. P. Abbott, L. J. Flewelling, R. W. Richardson, R. W. Dickey, E. L. Jester, et al., Saxitoxin puffer fish poisoning in the united states, with the first report of pyrodinium bahamense as the putative toxin source, *Environmental health perspectives* 114 (10) (2006) 1502–1507.
- [23] H. Klemick, C. Griffiths, D. Guignet, P. Walsh, Improving water quality in an iconic estuary: an internal meta-analysis of property value impacts around the chesapeake bay, *Environmental and resource economics* 69 (2) (2018) 265–292.
- [24] Chesapeake Bay Foundation, The economic benefits of cleaning up the chesapeake bay: A valuation of the natural benefits gained by implementing the chesapeake clean water blueprint, Tech. rep., Chesapeake Bay Foundation, Annapolis, MD (2014).  
URL <http://www.cbf.org/economicbenefits>
- [25] Chesapeake Bay Program, Chesapeake assessment and scenario tool (cast), version 2023, phase 6-[7.xx.x], <https://cast.chesapeakebay.net/>, chesapeake Bay Program Office; accessed [Month, Year]. (2024).
- [26] S. W. Ator, J. W. Brakebill, J. D. Blomquist, Sources, fate, and transport of nitrogen and phosphorus in the chesapeake bay watershed: An empirical model, Tech. rep., US Geological Survey (2011).

- [27] Chesapeake Bay Program, Cast model documentation, <https://cast.chesapeakebay.net/Documentation/ModelDocumentation>, accessed [Month, Year]. (2020).
- [28] I. D. Irby, M. A. Friedrichs, C. T. Friedrichs, A. J. Bever, R. R. Hood, L. W. Lanerolle, M. Li, L. Linker, M. E. Scully, K. Sellner, et al., Challenges associated with modeling low-oxygen waters in chesapeake bay: a multiple model comparison, *Biogeosciences* 13 (7) (2016) 2011–2028.
- [29] A. M. Farid, J. C. Little, Convergent anthropocene systems: Towards an agile, system-of-systems engineering approach, in: 2022 17th Annual System of Systems Engineering Conference (SOSE), IEEE, 2022, pp. 396–401.
- [30] S. W. Ator, A. M. Garcia, Application of sparrow modeling to understanding contaminant fate and transport from uplands to streams, *JAWRA Journal of the American Water Resources Association* 52 (3) (2016) 685–704.
- [31] C. F. Cerco, M. R. Noel, The 2017 chesapeake bay water quality and sediment transport model, Tech. rep., U.S. Army Engineer Waterways Experiment Station, Vicksburg, MS, accessed [Month, Year]. (2017).  
URL [https://www.chesapeakebay.net/documents/2017\\_WQSTM\\_Documentation\\_DRAFT\\_5-10-17.pdf](https://www.chesapeakebay.net/documents/2017_WQSTM_Documentation_DRAFT_5-10-17.pdf)
- [32] B. R. Bicknell, J. C. Imhoff, J. L. Kittle Jr, A. S. Donigian Jr, R. C. Johanson, Hydrological simulation program—fortran user’s manual for version 11, Environmental Protection Agency Report No. EPA/600/R-97/080. US Environmental Protection Agency, Athens, Ga (1997).
- [33] Chesapeake Bay Program, Chesapeake bay watershed model — application and calculation of nutrient and sediment loadings: Appendix i – model operations manual, Tech. rep., Chesapeake Bay Program Office, Annapolis, MD (August 1998).  
URL [https://www.chesapeakebay.net/files/documents/3\\_776.pdf](https://www.chesapeakebay.net/files/documents/3_776.pdf)
- [34] L. C. Linker, G. W. Shenk, R. L. Dennis, J. S. Sweeney, Cross-media models of the chesapeake bay watershed and airshed, Tech. rep., Chesapeake Bay Program Office, Annapolis, MD, available online: <https://www.chesapeakebay.net/> [Accessed Month Year] (1999).

- [35] D. E. Weller, M. E. Baker, Cropland riparian buffers throughout chesapeake bay watershed: Spatial patterns and effects on nitrate loads delivered to streams, *JAWRA Journal of the American Water Resources Association* 50 (3) (2014) 696–712.
- [36] J. S. Lefcheck, D. J. Wilcox, R. R. Murphy, S. R. Marion, R. J. Orth, Multiple stressors threaten the imperiled coastal foundation species eelgrass (*zostera marina*) in chesapeake bay, usa, *Global Change Biology* 23 (9) (2017) 3474–3483.
- [37] W. Ni, M. Li, J. M. Testa, Discerning effects of warming, sea level rise and nutrient management on long-term hypoxia trends in chesapeake bay, *Science of the Total Environment* 737 (2020) 139717.
- [38] J. M. Testa, R. R. Murphy, D. C. Brady, W. M. Kemp, Nutrient- and climate-induced shifts in the phenology of linked biogeochemical cycles in a temperate estuary, *Frontiers in Marine Science* Volume 5 - 2018 (2018). doi:10.3389/fmars.2018.00114.  
URL <https://www.frontiersin.org/journals/marine-science/articles/10.3389/fmars.2018.00114>
- [39] I. D. Irby, M. A. M. Friedrichs, F. Da, K. E. Hinson, The competing impacts of climate change and nutrient reductions on dissolved oxygen in chesapeake bay, *Biogeosciences* 15 (9) (2018) 2649–2668. doi:10.5194/bg-15-2649-2018.  
URL <https://bg.copernicus.org/articles/15/2649/2018/>
- [40] I. D. Irby, M. A. Friedrichs, Evaluating confidence in the impact of regulatory nutrient reduction on chesapeake bay water quality, *Estuaries and Coasts* 42 (1) (2019) 16–32.
- [41] S. W. Ator, J. D. Blomquist, J. S. Webber, J. G. Chanut, Factors driving nutrient trends in streams of the chesapeake bay watershed, *Journal of Environmental Quality* 49 (4) (2020) 812–834.
- [42] M. Amaya, A. Baran, C. Lopez-Morales, J. C. Little, A coupled hydrologic-economic modeling framework for scenario analysis, *Frontiers in Water* 3 (2021) 681553.

- [43] M. Amaya, F. Duchin, E. Hester, J. C. Little, Applying a coupled hydrologic-economic modeling framework: Evaluating alternative options for reducing impacts for downstream locations in response to upstream development, *Sustainability* 14 (11) (2022) 6630.
- [44] H. Abdolabadi, M. Amaya, J. C. Little, Intimate coupling of a hydrologic model with an economic input–output model using system dynamics, *Applied Water Science* 13 (3) (2023) 1–16.
- [45] O. L. de Weck, D. Roos, C. L. Magee, *Engineering Systems - Meeting Human Needs in a Complex Technological World*, The MIT Press, Cambridge, Massachusetts, 2011.
- [46] D. D. Walden, G. J. Roedler, K. J. Forsberg, R. D. Hamelin, T. M. Shortell, *Systems engineering handbook: A guide for system life cycle processes and activities*, Tech. rep., INCOSE (2015).
- [47] D. Hoyle, *ISO 9000 pocket guide*, Butterworth-Heinemann, Oxford ; Boston, 1998.  
URL <http://www.loc.gov/catdir/toc/els033/99163006.html>
- [48] W. C. Schoonenberg, I. S. Khayal, A. M. Farid, *A Hetero-functional graph theory for modeling interdependent smart City infrastructure*, Springer, 2019.
- [49] A. M. Farid, D. J. Thompson, W. Schoonenberg, A tensor-based formulation of hetero-functional graph theory, *Scientific Reports* 12 (1) (2022) 18805.
- [50] A. M. Farid, An engineering systems introduction to axiomatic design, in: A. M. Farid, N. P. Suh (Eds.), *Axiomatic Design in Large Systems: Complex Products, Buildings & Manufacturing Systems*, Springer, Berlin, Heidelberg, 2016, Ch. 1, pp. 1–47.  
URL <http://dx.doi.org/10.1007/978-3-319-32388-6>
- [51] W. C. Schoonenberg, A. M. Farid, Hetero-functional Network Minimum Cost Flow Optimization, *Sustainable Energy Grids and Networks* 31 (100749) (2022) 1–18.  
URL <https://doi.org/10.1016/j.segan.2022.100749>

- [52] A. M. Farid, Product Degrees of Freedom as Manufacturing System Reconfiguration Potential Measures, *International Transactions on Systems Science and Applications – invited paper* 4 (3) (2008) 227–242.  
URL <http://liines.net/resources/Journals/IEM-J04.pdf>
- [53] I. S. Khayal, A. M. Farid, Architecting a system model for personalized healthcare delivery and managed individual health outcomes, *Complexity* 2018 (2018) 1–24.
- [54] W. C. Schoonenberg, A. M. Farid, A dynamic model for the energy management of microgrid-enabled production systems, *Journal of cleaner production* 164 (2017) 816–830.
- [55] A. M. Farid, D. C. McFarlane\*, Production degrees of freedom as manufacturing system reconfiguration potential measures, *Proceedings of the Institution of Mechanical Engineers, Part B (Journal of Engineering Manufacture) – invited paper* 222 (B10) (2008) 1301–1314.  
doi:10.1243/09544054JEM1056.  
URL <http://dx.doi.org/10.1243/09544054JEM1056>
- [56] I. S. Khayal, A. M. Farid, A dynamic system model for personalized healthcare delivery and managed individual health outcomes, *IEEE Access* 9 (2021) 138267–138282.
- [57] I. S. Khayal, A. M. Farid, Axiomatic Design Based Volatility Assessment of the Abu Dhabi Healthcare Labor Market, *Journal of Enterprise Transformation* 5 (3) (2015) 162–191.  
URL <http://dx.doi.org/10.1080/19488289.2015.1056449>
- [58] F. M. White, *Fluid mechanics*, 3rd Edition, McGraw-Hill, New York, 1994.
- [59] A. M. Farid, I. S. Khayal, *The Hetero-functional Graph Theory Toolbox: A Practical Handbook*, In preparation. Early version at: <https://arxiv.org/abs/2005.10006> (2025).  
URL <https://arxiv.org/abs/2005.10006>
- [60] D. Thompson, A. M. Farid, A Reference Architecture for the American Multi-Modal Energy System, *Journal of Industrial Information Integration* 36 (2023) 100521–100531.  
URL <https://doi.org/10.1016/j.jii.2023.100521>

- [61] D. Thompson, A. M. Farid, A hetero-functional graph structural analysis of the american multi-modal energy system, *Sustainable Energy, Grids, and Networks* 38 (1) (2024) 101254–101269.  
URL <https://doi.org/10.1016/j.segan.2023.101254>
- [62] D. Thompson, A. M. Farid, Hetero-functional network simulation and optimization: A hydrogen-natural gas network example, in: *CSIRO Invited Seminar*, Clayton, Victoria, Australia, 2022.
- [63] D. Thompson, W. C. Schoonenberg, A. M. Farid, A Hetero-functional Graph Resilience Analysis of the Future American Electric Power System, *IEEE Access* 9 (2021) 68837–68848.  
URL <https://doi.org/10.1109/ACCESS.2021.3077856>
- [64] D. Thompson, W. C. Schoonenberg, A. M. Farid, A Hetero-functional Graph Analysis of Electric Power System Structural Resilience, in: *IEEE Innovative Smart Grid Technologies Conference North America*, Washington, DC, United states, 2020, pp. 1–5.  
URL <http://dx.doi.org/10.1109/ISGT45199.2020.9087732>
- [65] W. C. Schoonenberg, A. M. Farid, Modeling Smart Cities with Hetero-functional Graph Theory, in: *2017 IEEE International Conference on Systems, Man, and Cybernetics (SMC2017), Intelligent Industrial System Special Session*, Vol. 1, Banff, Canada, 2017, pp. 1–10.  
URL <http://dx.doi.org/10.1109/SMC.2017.8122848>
- [66] W. C. Schoonenberg, A. M. Farid, Hetero-functional graph theory for interdependent smart city infrastructures, in: *2018 IEEE Smart Cities Workshop*, 2018.
- [67] W. C. Schoonenberg, I. S. Khayal, A. M. Farid, *A Hetero-functional Graph Theory for Modeling Interdependent Smart City Infrastructure*, Springer, Berlin, Heidelberg, 2019.  
URL <http://dx.doi.org/10.1007/978-3-319-99301-0>
- [68] I. S. Khayal, A. M. Farid, Architecting a System Model for Personalized Healthcare Delivery and Managed Individual Health Outcomes, *Complexity* 1 (1) (2018) 1–25.  
URL <https://doi.org/10.1155/2018/8457231>

- [69] I. S. Khayal, A. M. Farid, A Dynamic System Model for Personalized Healthcare Delivery and Managed Individual Health Outcomes, *IEEE Access* 9 (2021) 138267–138282.  
URL <https://dx.doi.org/10.1109/ACCESS.2021.3118010>
- [70] T. Kelepouris, C. Y. Wong, A. M. Farid, A. K. Parliad, D. C. McFarlane\*, Towards a reconfigurable supply network model, in: *Intelligent Production Machines and Systems – 2nd I\*PROMS Virtual International Conference 3–14 July 2006*, Elsevier, Online, 2006, pp. 1–6.  
URL <http://www.sciencedirect.com/science/article/pii/B9780080451572500857>
- [71] W. C. Schoonenberg, A. M. Farid, A Dynamic Model for the Energy Management of Microgrid-Enabled Production Systems, *Journal of Cleaner Production* 1 (1) (2017) 1–10.  
URL <https://dx.doi.org/10.1016/j.jclepro.2017.06.119>
- [72] A. M. Farid, D. J. Thompson, W. Schoonenberg, A tensor-based formulation of hetero-functional graph theory, *Scientific Reports* 12 (1) (2022) 18805.
- [73] S. Yang, K. Choi, K. Paik, Power law between the apparent drainage density and the pruning area, *Hydrology and Earth System Sciences* 28 (14) (2024) 3119–3132. doi:10.5194/hess-28-3119-2024.  
URL <https://hess.copernicus.org/articles/28/3119/2024/>
- [74] K. Beven, A. Binley, The future of distributed models: model calibration and uncertainty prediction, *Hydrological processes* 6 (3) (1992) 279–298.
- [75] H. V. Gupta, S. Sorooshian, P. O. Yapo, Toward improved calibration of hydrologic models: Multiple and noncommensurable measures of information, *Water Resources Research* 34 (4) (1998) 751–763.
- [76] A. Buda, Surface-runoff generation and forms of overland flow, in: *Mountain and Hillslope Geomorphology*, Elsevier Inc., 2013, pp. 73–84.
- [77] A. R. Buda, P. J. Kleinman, G. W. Feyereisen, D. A. Miller, P. G. Knight, P. J. Drohan, R. B. Bryant, Forecasting runoff from pennsylvania landscapes, *Journal of Soil and Water Conservation* 68 (3) (2013) 185–198.

- [78] B. Dari, V. D. Nair, A. N. Sharpley, P. Kleinman, D. Franklin, W. G. Harris, Consistency of the threshold phosphorus saturation ratio across a wide geographic range of acid soils, *Agrosystems, Geosciences & Environment* 1 (1) (2018) 1–8.
- [79] A. R. Buda, P. J. Kleinman, M. Srinivasan, R. B. Bryant, G. W. Feyerisen, Factors influencing surface runoff generation from two agricultural hillslopes in central pennsylvania, *Hydrological Processes: An International Journal* 23 (9) (2009) 1295–1312.